SNOW ON ANTARCTIC SEA ICE

Robert A. Massom,[1] Hajo Eicken,[2] Christian Haas,[3] Martin O. Jeffries,[2]
Mark R. Drinkwater,[4,5] Matthew Sturm,[6] Anthony P. Worby,[1,7] Xingren Wu,[1,7]
Victoria I. Lytle,[1,7] Shuki Ushio,[8] Kim Morris,[2] Phillip A. Reid,[1,9]
Stephen G. Warren,[10] and Ian Allison[1,7]

Abstract. Snow on Antarctic sea ice plays a complex and highly variable role in air-sea-ice interaction processes and the Earth's climate system. Using data collected mostly during the past 10 years, this paper reviews the following topics: snow thickness and snow type and their geographical and seasonal variations; snow grain size, density, and salinity; frequency of occurrence of slush; thermal conductivity, snow surface temperature, and temperature gradients within snow; and the effect of snow thickness on albedo. Major findings include large regional and seasonal differences in snow properties and thicknesses; the consequences of thicker snow and thinner ice in the Antarctic relative to the Arctic (e.g., the importance of flooding and snow-ice formation); the potential impact of increasing snowfall resulting from global climate change; lower observed values of snow thermal conductivity than those typically used in models; periodic large-scale melt in winter; and the contrast in summer melt processes between the Arctic and the Antarctic. Both climate modeling and remote sensing would benefit by taking account of the differences between the two polar regions.

1. INTRODUCTION

At maximum extent each year (September–October), sea ice covers a vast area of the Southern Ocean (~19 million km^2), attaining latitudes as far north as ~55°S [*Gloersen et al*., 1992]. In so doing, it profoundly alters the exchange of energy and mass between ocean and atmosphere and forms an integral part of the global climate system. These effects are significantly amplified by the presence of an insulative snow cover which is itself highly variable in thickness and properties. Persistently strong winds redistribute the snow, and its properties constantly evolve as a result of a range of metamorphism processes.

Because of its low thermal conductivity (about an order of magnitude lower than that of sea ice), snow greatly modifies the sea ice thermodynamically, affecting seasonal accretion [*Maykut and Untersteiner*, 1971] and ablation rates. The latter in turn affect the structure and dynamics of the underlying ocean via the input of brine [*Gordon and Huber*, 1990] and freshwater [*Fahrbach et al*., 1991], respectively. Because of its high albedo compared with that of sea ice, snow dominates the surface shortwave energy exchange [*Maykut*, 1986]. By smoothing the ice surface, snow greatly modifies the ice-air drag coefficient [*Andreas et al*., 1993] and the bulk transfer coefficients for latent and sensible heat [*Andreas*, 1987]. It also has a first-order effect on the microwave properties of the surface, leading to ambiguity in retrievals of sea-ice type and concentration from satellite data [e.g., *Comiso*, 1983; *Drinkwater et al*., 1995; *Lohanick*, 1990]. Snow also reflects photosynthetically active radiation (PAR) and so reduces the amount available to sea-ice algae [*Sullivan et al*., 1985].

Modeling studies have shown that the Antarctic sea-ice zone is highly sensitive to global climate change [*Mitchell et al*., 1990; *Wu et al*., 1999], with snow on sea ice enhancing its sensitivity [*Eicken et al*., 1994]. This is an important factor given that some models predict enhanced net precipitation as a result of global warming [e.g., *Manabe et al*., 1991]. Enhanced snow accumulation on sea ice may result in an overall cooling effect on global climate [*Ledley*, 1991]. However, while the importance of sea ice is well established, detailed field studies

[1] Antarctic Cooperative Research Centre, c/o University of Tasmania, Hobart, Tasmania, Australia.
[2] Geophysical Institute, University of Alaska Fairbanks, USA.
[3] Alfred-Wegener-Institut für Polar-und Meeresforschung, Bremerhaven, Germany.
[4] Oceans/Sea-Ice Unit, European Space Agency, Noordwijk, Netherlands.
[5] Formerly at NASA Jet Propulsion Laboratory, California Institute of Technology, Pasadena, California, USA.
[6] U.S. Army Cold Regions Research and Engineering Laboratory–Alaska, Fort Wainwright, Alaska, USA.
[7] Also at Australian Antarctic Division, Kingston, Tasmania, Australia.
[8] National Institute of Polar Research, Tokyo, Japan.
[9] Now at Climatic Research Unit, University of East Anglia, Norwich, England.
[10] Department of Atmospheric Sciences, University of Washington, Seattle, Washington, USA.

Reviews of Geophysics, 39, 3 / *August 2001*
pages 413–445
8755-1209/01/2000RG000085*$15.00*
Paper number 2000RG000085

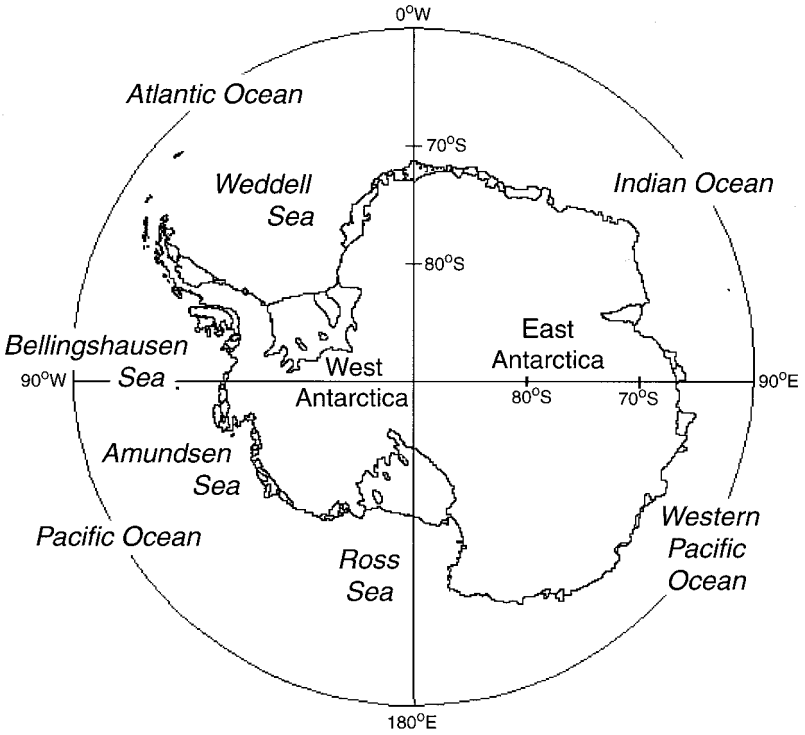

Figure 1. Map of Antarctica, showing the locations of the different seas and oceans discussed in the text.

on snow distribution and properties have only been conducted in the past 5–10 years. These studies are beginning to establish the full significance of snow on Antarctic sea ice as a key component of the global climate system.

In this paper we review the major findings. Section 2 is a summary of snow data from five Antarctic sectors (designated by *Gloersen et al*. [1992]), namely, the Weddell Sea (20°E–60°W), the Indian Ocean (20°E–90°E), the western Pacific Ocean (90°E–160°E), the Ross Sea (160°E–140°W), and the Bellingshausen and Amundsen Seas (140°W–60°W), as shown in Figure 1. The Indian and western Pacific Ocean sectors are collectively referred to as the East Antarctic sector. Section 3 assesses the significance of snow in the air-sea-ice interaction system. New findings have significant implications for modeling (both physical and biological) and remote-sensing studies of Antarctic sea ice. Gaps in our current knowledge are identified. Finally, the possible enhanced role of snow under global warming conditions is examined. Throughout, snow is described using the combined morphological and process-oriented classification of snow types of *Colbeck et al*. [1990], and sea ice is described using the World Meteorological Organization (WMO) nomenclature [*WMO*, 1971].

2. PHYSICAL PROPERTIES

2.1. Snow Thickness Distribution

Snow thickness (z_s) is typically measured directly in situ or by routine hourly visual estimates from ships in transit. At present, no remote-sensing technique can provide reliable measurements from space, although promising methods are under development [e.g., *Arrigo et al*., 1996; *Markus and Cavalieri*, 1998].

2.1.1. Snow thickness distribution on pack ice. Because of persistently strong winds over Antarctic sea ice, typically immediately following precipitation events [*Massom et al*., 1997, 1998], windblown redistribution is a key factor affecting the snow thickness distribution. Redistribution of dry, unconsolidated snow occurs at wind speeds of $>6-8$ m s^{-1} [*Andreas and Claffey*, 1995]. As a result, thickness may not be directly related to either the frequency or duration of snowfall.

Mean snow thicknesses are given in Table 1 and vary widely (from 0.02 to 0.49 m) both seasonally and regionally due to differences in precipitation regimes (see section 3.5) and the age of the underlying ice. Similar regional and seasonal differences are noted in frequency distributions from different sectors, as shown in Figure 2. Snow thicker than ~0.25 m represents drifted snow or, in the case of snow thicker than ~1.0 m, multiyear accumulation on perennial floes 3–10 m thick [*Jeffries et al*., 1994a; *Massom et al*., 1997, 1998; *Wadhams et al*., 1987]. For comparison, snow thickness on Arctic multiyear ice attains a thickness of 0.26–0.42 m at the end of the accumulation season in May [*Warren et al*., 1999].

The winter distributions in Figures 2a, 2c, and 2e are similar, with few data from the thin class (0–0.05 m), as only a small proportion of the pack comprised thin ice. That the winter Weddell Sea distribution (in Figure 2b) resembles the Ross Sea autumnal distribution (in Figure 2d) is because the new pancake ice formation dominated

TABLE 1. Mean Snow Thicknesses Measured Over Antarctic Sea Ice, From Drill-Hole Measurements (Unless Otherwise Stated)[a]

Region	*Season, Year*[b]	*Mean and 1σ, m*	*Range,*[c] m	*n*	*Reference*
		Indian and Western Pacific Oceans			
62°–110°E, 58°–66°S	spring 1988	···	0.05–0.15	···	*Allison et al.* [1993]
64°–106°E	spring 1991	0.10 ± 0.13	0.01–0.45	47	*Worby and Massom* [1995]
62°–102°E	spring 1992	0.12 ± 0.16	0.01–0.76	67	*Worby and Massom* [1995]
75°–150°E	spring 1994	0.15 ± 0.20	0.05–1.40	113	*Worby and Massom* [1995]
139°–141°E, 144°–150°E	autumn 1993	0.06 ± 0.12	0.00–1.50	186	*Worby and Massom* [1995]
138°–142°E	winter 1995	0.13 ± 0.09	0.02–2.01	794	*Massom et al.* [1998]
138°–142°E	winter 1995	0.13 ± 0.12 (SO)	0.01–0.90	165	*Worby et al.* [1998]
		Bellingshausen, Amundson, and Ross Seas			
161°–168°E	summer 1990–1991	0.02 ± 0.05	0.01–0.23	100	*Jeffries and Weeks* [1993]
164.5°E, 75.5°S	summer 1991	0.16 ± 0.03 (OM)	0.10–0.27	56 (AA)	*Danielson and Jeffries* [1992]
167°E, 78°S,	summer 1992	0.18 ± 0.03 (FI)	0.125–0.34	50	*Veazey et al.* [1994]
102°W, 75°S		0.27 ± 0.04 (FI)	0.21–0.36	31	
165°E	summer 1965		0.02–0.60 (FI)	···	*Paige and Lee* [1967]
75°W	late summer 1994	0.45 ± 0.16	0.12–0.69	35	*Haas et al.* [1996]
85°W	late summer 1994	0.29 ± 0.24	0.05–0.98	75	*Haas et al.* [1996]
105°W	late summer 1994	0.46 ± 0.30	0.05–0.78	19	*Haas et al.* [1996]
120°W	late summer 1994	0.49 ± 0.26	0.05–1.01	41	*Haas et al.* [1996]
70°–160°W	summer/autumn 1992	0.34 ± 0.15	0.16–0.70	100	*Jeffries et al.* [1994a]
70°–160°W	summer/autumn 1992	0.34 ± 0.15	0.17–1.98	16	*Jeffries et al.* [1994b]
160°E–100°W	autumn 1992	0.27 ± 0.04 (FI)	0.21–0.36	31	*Veazey et al.* [1994]
165°–180°W	autumn/winter 1995	0.15 ± 0.11	0.00–0.83	3,670	*Jeffries and Adolphs* [1997]
165°–180°W	autumn/winter 1995	0.11 ± 0.10 (SO)	0.00–1.50	11,114	
109°–171°W	winter/spring 1994	0.13 ± 0.07	0.05–0.32	2,413	*Sturm et al.* [1998]
68°–80°W,	autumn/winter 1999	0.03 ± 0.03	···	404	S. Stammerjohn (personal communication, 2000)
62°–69°S		0.04 ± 0.03 (SO)		109	
109°–171°W	winter/spring 1994	0.29 ± 0.09	0.00–1.75	7,583	*Sturm et al.* [1998]
109°–171°W	winter/spring 1994	0.27 ± 0.09	0.11–0.79	2,227	*Jeffries et al.* [1998b]
109°–171°W	winter/spring 1994	0.17 ± 0.10 (SO)	0.00–0.75	9,125	*Jeffries et al.* [1998b]
75°–110°W	winter/spring 1993	0.23 ± 0.16 (SO)	0.03–0.82	1,113	*Jeffries et al.* [1994b]
75°–110°W	winter/spring 1993	0.19 ± 0.12 (SO)	0.00–1.00	4,071	*Worby et al.* [1996b]
80°–110° and 155°–180°W	winter/spring 1995	0.22 ± 0.09	0.07–0.33	2,882	*Sturm et al.* [1995, 1998]
		Weddell Sea			
0°, 58°–60°S	spring 1981	0.30	···	26	*Clarke and Ackley* [1982]
46°–54°W, 59°–64°S	spring 1988	0.31	0.08–0.50	1,553	*Eicken et al.* [1994], *Lange and Eicken* [1991]
0°–55°W	spring 1989	0.26 ± 0.23	0.01–1.29	5,339	*Eicken et al.* [1994]
	spring 1989	0.18	0.01–0.80	2,650	*Meese et al.* [1990]
36°–40°W	spring/summer 1983	0.41 (SO)	···	···	*Comiso and Sullivan* [1986]
40°W, 64°–74°S	summer/autumn 1980	···	0.02–0.56	77	*Gow et al.* [1987]
5°E–55°W	autumn/winter 1992	0.28 ± 0.15	0.08–0.62	4,000	*Fisher and Lytle* [1998]
5°E–55°W	autumn/winter 1992	0.32 ± 0.31 (SO)	0.01–1.00	173	V. Lytle (unpublished data, 2001)
5°E–20°W	autumn/winter 1994	0.12 ± 0.06	0.01–0.63	1,830	
5°E–20°W	autumn/winter 1994	0.10 ± 0.06 (SO)	0.01–1.00	360	V. Lytle (unpublished data, 2001)
5°W–7°E, 56°–70°S	winter 1986	0.11	···	4,238	*Wadhams et al.* [1987]
0°–50°W	winter 1992	0.14 ± 0.17	0.01–0.95	582	*Massom et al.* [1997]
0°–50°W	winter 1992	0.12 ± 0.14	···	386	*Eicken et al.* [1994]
20°–40°W	late summer 1997	0.22 ± 0.15	0.01–1.20	716	*Haas et al.* [1998]
45°–57°W	late summer 1997	0.11 ± 0.14	0.01–0.93	783	*Haas et al.* [1998]

[a]AA denotes a range of area averages; SO denotes ship observations; FI denotes fast ice; and OM denotes measurements from one floe only.
[b]Spring means September–November, summer means December–February, autumn means March–May, and winter means June–August.
[c]Minimum does not include snow on nilas, which would have zero thickness.

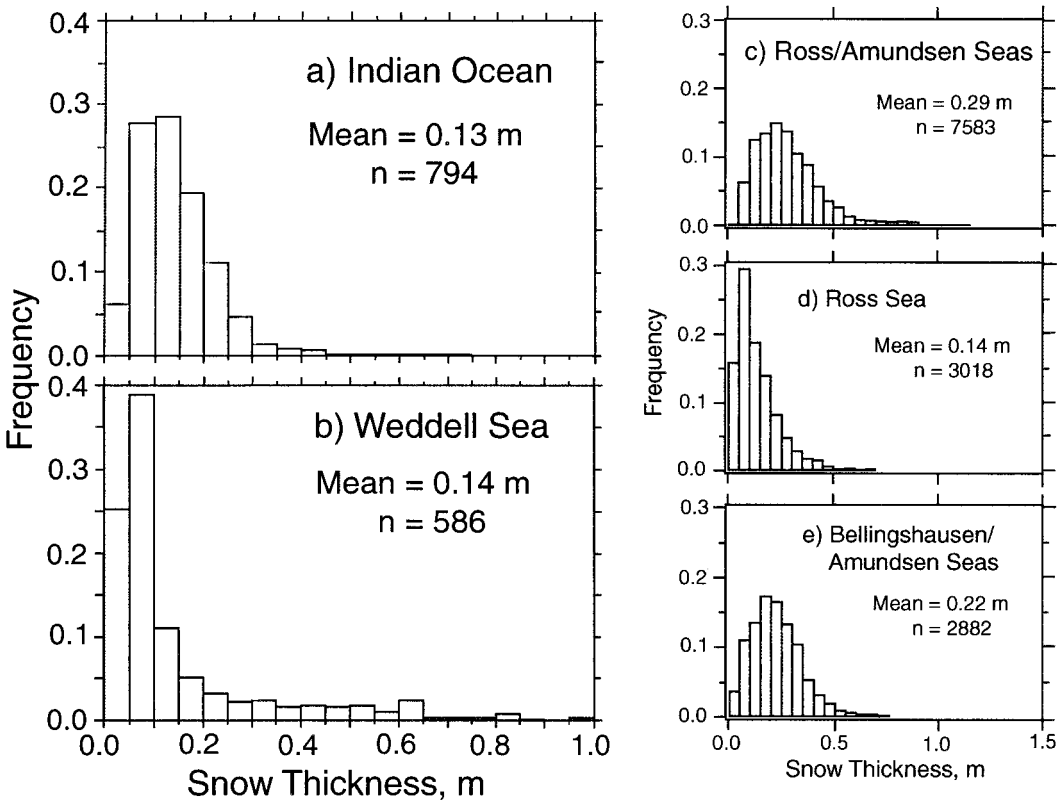

Figure 2. Frequency distributions of snow thickness from different Antarctic sectors: (a) Indian Ocean, winter 1995 [after *Massom et al.*, 1998]; (b) Weddell Sea, winter 1992 [after *Massom et al.*, 1997]; (c) Amundsen and Ross Seas, winter–spring 1994; (d) Ross Sea, autumn 1995; and (e) Bellingshausen and Ross Seas, winter 1995. Figures 2c–2e are after *Sturm et al.* [1998].

the early part of the former cruise. In autumn, the snow (and ice) had yet to attain its maximum thickness. Seasonal and regional variability is further discussed in section 3.1. Relatively few snow thickness data have been collected in summer.

2.1.2. Snow thickness distribution on fast ice. Fast ice is sea ice that forms at, and remains attached ("fast") to, the coast or grounded icebergs. At its maximum extent (in November), Antarctic fast ice covers an estimated 550,000 km^2 [*Fedotov et al.*, 1998]. While virtually no snow accumulates in fast-ice regions affected by katabatic winds (strong, persistent winds that cascade down off the Antarctic continent), significant accumulation can occur in other regions [*Kawamura et al.*, 1995; *Ushio and Takizawa*, 1993]. Data from one transect are shown in Table 2. While relatively low accumulations are measured at sites nearest the coast (transect L0), snow thickness increases significantly with increasing distance offshore (attaining thicknesses up to 1.65 m). Farther to the east, the average snow thickness ranges from 0.6 to 1.0 m on the "seaward" fast-ice zone (6–15 km offshore), where the wind weakens and accumulation occurs in the form of snow blown off the continent as well as precipitation from cyclones [*Fedotov et al.*, 1998].

TABLE 2. Snow Thickness (z_s) and Sea-Ice Thickness (z_i) Data From Stations on Fast Ice in Lützow-Holm Bay, East Antarctica [After *Kawamura et al.*, 1995][a]

Date	*L0*		*L1*		*L2*		*L3*		*L4*		*L5*	
	z_s	z_i	z_s	z_i	z_s	z_i	z_s	z_i	z_s	z_i	z_s	z_i
May 1990	···	···	0.11	1.44	0.39	2.20	0.63	2.15	0.72	2.20	···	···
Aug. 1990	···	···	0.15	1.70	0.70	2.50	0.97	2.13	1.20	2.13	1.40	2.13
Oct. 1990	···	···	0.29	1.98	1.05	2.22	1.39	2.24	1.59	2.37	1.65	2.12
April 1991	0.05	0.72	0.05	1.45	0.10	2.10	0.35	3.03	0.58	3.16	0.47	2.88
Aug. 1991	0.20	1.34	0.22	1.74	0.36	2.15	0.86	3.25	0.92	2.81	1.12	2.97
Oct. 1991	0.15	1.60	0.20	2.04	0.53	2.36	0.98	3.25	1.13	2.86	1.42	2.80
Jan. 1992	···	···	···	···	···	···	0.53	3.38	···	···	···	···

[a]Transect L0 to L5 runs offshore from east to west, from ~69°16′S, 39°30′E to ~69°17′S, 38°30′E.

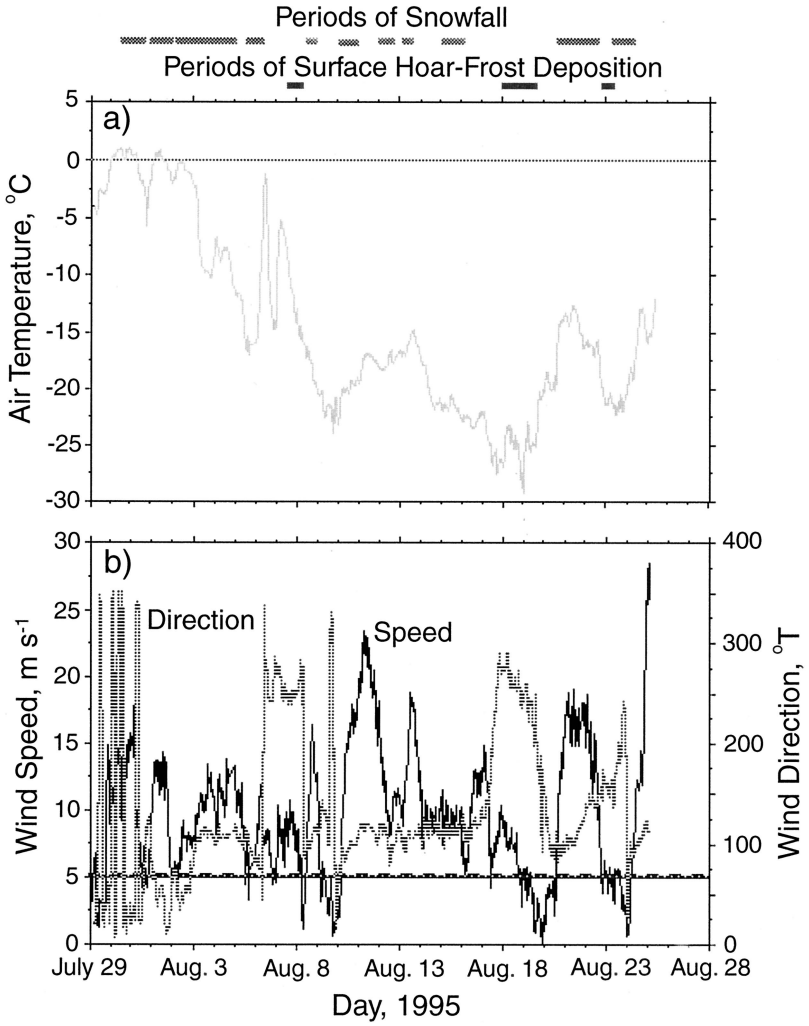

Figure 3. Time series of (a) near-surface air temperature and (b) wind speed and direction measured from the R/V *Aurora Australis* while in the pack ice, August 1995, off East Antarctica. The horizontal dashed line denotes the approximate wind speed above which aeolian transport of unconsolidated snow occurs. Periods of snowfall and surface hoar-frost deposition are also marked. After *Massom et al.* [1998].

Petrov [1967] found the maximum snow depth 13 km offshore of Mirny.

2.2. Snow Properties

2.2.1. Snow stratigraphic and textural characteristics. The temporal evolution of an accumulating snow cover is highly complex. At the microscopic level, processes of crystalline modification, collectively referred to as snow metamorphism, occur immediately after deposition and significantly modify the snow texture. Dry-snow metamorphism, which is driven by water vapor movement in pores, is subdivided into (1) equitemperature (ET) and (2) temperature-gradient (TG) processes [*Colbeck*, 1982; *Granberg*, 1998; *Sommerfeld and LaChapelle*, 1970]. These processes are also known as "kinetic" and "equilibrium" growth, respectively [*Colbeck*, 1982]. In ET metamorphism, snowflakes rapidly transform into an aggregate of rounded smooth grains in a snowpack that is roughly isothermal; it is also termed destructive metamorphism, as it effectively destroys the crystal structure. This process is most important during the early stages of snow deposition, when wind also mechanically fragments and compacts the snow to create a medium- to high-density surface layer known as "wind slab." In addition to crystal rounding, the overall effect of ET metamorphism is to reduce the snow surface to volume ratio, to increase the density (by filling in pore spaces), to round the grains, and to increase the snow strength (by building bonds between crystals). Temperature-gradient metamorphism occurs where a large temperature gradient (generally less than about $-10°C$ m^{-1}), set up by the insulative effect of the snow cover, promotes the rapid upward migration of water vapor through the snowpack. Significant crystal enlargement occurs by this kinetic growth (hence the alternative term constructive metamorphism), and the formation of more complex (angular and faceted) crystals takes place. This

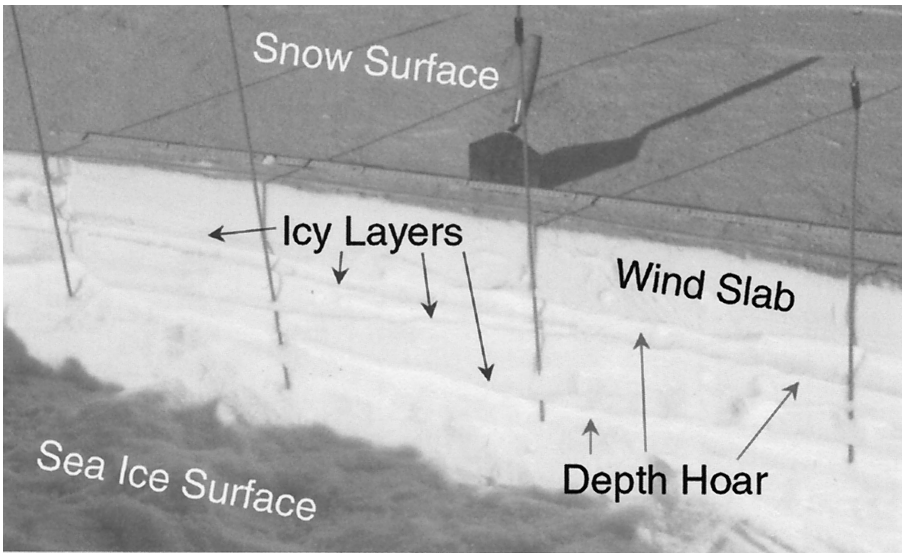

Figure 4. Photograph of a typical winter snow pit (thickness 0.25 m) from the Amundsen Sea, September 1994, showing distinct layering.

produces a lower-density snow, with poor intercrystalline bonding. Wet-snow metamorphism occurs when liquid water is present (due to melt and/or the incursion of seawater). Under these conditions, rates of metamorphism tend to accelerate, with small grains being preferentially destroyed and large grains becoming rounded. Subsequent refreezing results in a coarse-grained, icy snow characterized by large, bonded grain clusters. In the case of snow on Antarctic sea ice, the introduction of brine into the snow further complicates these processes (see section 2.2.4).

Snow-crystal metamorphism, in combination with additional snow accumulation, intermittent meltwater percolation, and upward migration of brine, results in the formation of a complex snowpack. Another key factor is the interplay of environmental variables (local topography, temperature, wetness, solar radiation, wind) both during and after deposition. Weather conditions in the Antarctic sea-ice zone are highly dynamic and variable, with periods of high temperatures (to ~0°C) in winter and strong winds often accompanying snowfall [*Massom et al*., 1997], as is shown in Figure 3. As a result, snow on Antarctic sea ice by no means forms a uniform slab. Rather, it comprises numerous layers with different physical characteristics (Figure 4) [*Massom et al*., 1997; *Sturm et al*., 1998]. Particularly complex stratigraphies are observed in older snow covers on multiyear or fast ice [*Massom et al*., 1998].

The six dominant snow classes in winter are (1) new and recent snow, (2) soft and moderate slab, (3) hard slab, (4) faceted snow and depth hoar, (5) icy layers, and (6) saline slush [*Massom et al*., 1998; *Sturm et al*., 1998]. Photomicrographs of four types are shown in Figure 5. Percentages of different snow types observed from the Indian Ocean [*Massom et al*., 1998] and the Bellingshausen, Amundsen, and Ross Seas [*Sturm et al*., 1998] are presented in Table 3. Typical mean grain size and density as a function of snow type in winter are given in Table 4. Grain size is measured from vertical profiles [e.g., *Massom et al*., 1998] and by sieving bulk snow samples [*Sturm*, 1991]. The "grain size" we report here is for the longest dimension; for a rounded crystal, it is the diameter. For new and recent snow, density and grain size depend upon the conditions during deposition [*Colbeck et al*., 1990]. *Sturm et al*. [1998] suggest that the relatively high air temperatures and persistent winds that often accompany snowfall [*Drinkwater*, 1995; *Massom et al*., 1998] account for the relative abundance of soft to moderate slabs with a fine-grained texture (Table 3). They note a near-absence of hard slabs like those commonly observed in Arctic Alaska under similar wind conditions but significantly lower temperatures [*Benson and Sturm*, 1993].

While recent snow covers are characterized by angular (mechanically fragmented) or rounded crystal forms, significantly larger crystals in the form of faceted snow and depth hoar dominate in older and colder snow covers [*Massom et al*., 1997, 1998], as is shown in Tables 3 and 4. Depth-hoar formation occurs at temperature gradients of about $-10°$ to $-25°\text{C m}^{-1}$ [*Akitaya*, 1974; *Armstrong*, 1980; *Colbeck*, 1982]. Bulk temperature gradient (∇T) is assumed to be vertical and linear and is defined by $(T_s - T_i)/z_s$, where T_s is the snow-surface temperature and T_i is the snow/ice interface temperature. New, thin snow covers soon exhibit textural complexity as a result of rapid depth-hoar formation due to steep temperature gradients [*Massom et al*., 1998]. The greatest proportions of depth hoar occur in autumn (Table 3) and are probably linked to the larger (negative) ∇T across a thinner snowpack (see section 3.4.1.).

Another important feature is the prevalence of icy layers, which are present in all seasons (Table 3). On the

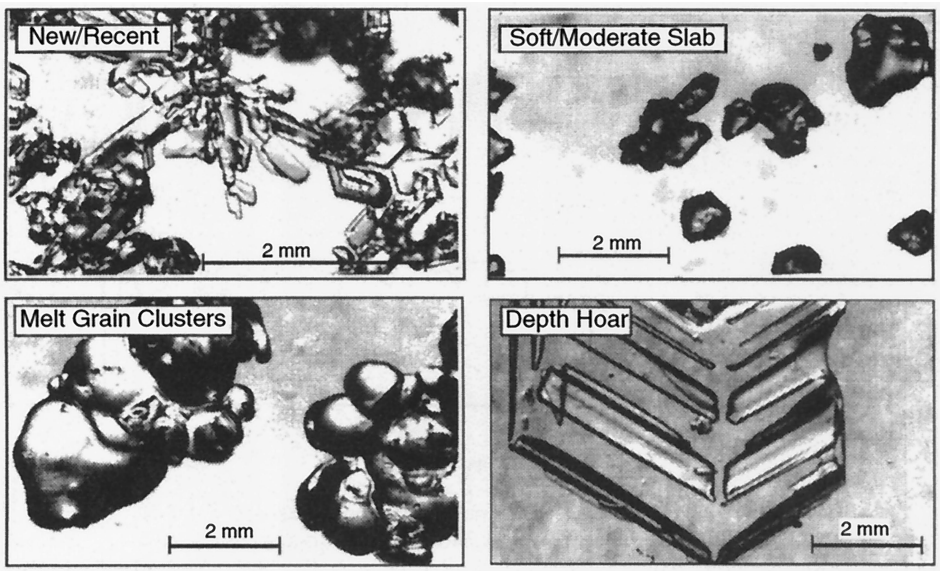

Figure 5. Photomicrographs of the four primary snow types encountered in late winter 1994 in the Bellingshausen and Ross Seas. From *Sturm et al*. [1998].

snow surface, wind and polycrystalline crusts form rapidly due to synoptic variability in T_{air} and relative humidity, the frequency of high winds, and even sleet/rain freezing on hitting the surface at lower latitudes (even in winter) [*Massom et al*., 1997; *Sturm et al*., 1998]. Surface wind-glazing occurs by the formation of regelation ice films on the snow surface following the kinetic heating of wind-driven saltating drift snow [*Goodwin*, 1990]. Other icy snow surface features, including glaze, occur by radiational effects [*Colbeck*, 1991]. By these processes, snow microrelief features such as hoarfrost flowers transform into icy rippled and "nubbly" layers consisting of irregular lumps of ice, 0.01–0.02 m high and spaced every few centimeters. Upwind faces of sastrugi are particularly susceptible to crust formation [*Massom et al*., 1997].

Although surface crusts constitute only a small fraction of the total snow volume (e.g., <3% in August 1995 in East Antarctica [*Massom et al*., 1998]), they cover large areas and play a significant role in "locking up" the snow and reducing aeolian erosion, redistribution, and snow sublimation [*Eicken et al*., 1994; *Massom et al*., 1997]. They probably also limit wind pumping [*Waddington et al*., 1996]. When buried, crusts intercept meltwater intermittently percolating downward during occasional warm periods [*Colbeck*, 1991], even in winter [*Jeffries et al*., 1997b; *Massom et al*., 1998; *Sturm et al*., 1998]. This meltwater spreads out laterally and subsequently refreezes, and the resultant icy layers can attain thicknesses of 0.05 m, but are commonly less than 0.01 m, and extend horizontally for distances of meters, having a significant effect on polarization in passive microwave remote sensing [*Garrity*, 1992]. Horizontal icy layers also form largely impermeable barriers to the upward flux of water vapor in colder snow, leading to enhanced depth-hoar formation underneath [*Colbeck*, 1991]. Where meltwater percolates downward through the snowpack and

TABLE 3. The Percentage of Different Snow Types Sampled on Seven Different Antarctic Sea-Ice Cruises.

Time Region[a]	*Spring '94 East Ant.*	*Spring '94 Am./Ross*	*Autumn '93 East Ant.*	*Autumn/ Winter '95 Ross*	*Winter '95 East Ant.*	*Winter/ Spring '94 Bell./Am.*	*Winter/ Spring '95 Bell./Ross*
Number of snow pits	10	164	16	73	46	58	45
% Icy (6a, 8a to 8c, 9d, 9c)	16	20	18	26	18	9	46
% New and recent (1a–1e, 2a, 2b)	11	14	12	8	23	30	4
% Soft and moderate slab (3b, 3c)	7	23	7	10	8		13
% Hard slab (3a)	9	6	11	0	9		0
% Faceted/Depth hoar (4a–4c, 5a–5c)	54	31	48	47	39	55	29
% Slush (6c)	3	6	4	9	3	6	8
Mean depth, m	0.15	0.28	0.17	0.14	0.13	0.20	0.22
Mean ∇T, °C m^{-1}	···	−23	−66	−82	−47 (n = 751)	−41	−44

[a] Classifications (6a, etc.) are according to *Colbeck et al. [1990].*

TABLE 4. Mean Grain Size and Density as a Function of the Major Snow Types, From Sieving of Snow in Winter in the Amundsen and Ross Seas, With 1σ [After *Sturm et al.*, 1998][a]

Snow Type	*Grain Size, mm*	n[a]	*Snow Density, kg m^{-3}*
New/recent snow	1.1 ± 0.6	2	310
Soft-moderate slabs	1.1 ± 0.4	21	340
Hard slabs	0.9 ± 0.3	4	410
Depth hoar	2.0 ± 0.9	29	290
Melt-grain clusters	1.3 ± 0.6	8	350

[a]Number of snow pits.

refreezes on the sea ice surface, "superimposed" ice forms (see section 3.2.2).

Snow texture is also intermittently altered by a wetting or dampening of the snow by melting, flooding with seawater, or the incorporation of brine from the underlying sea-ice surface. Flooding creates large, poorly bonded rounded crystals in the form of slush [*Colbeck et al.*, 1990]. Above the slush layer, capillary "wicking" of seawater upward into the snow mass significantly alters the snow texture to a height of 0.1–0.2 m [*Massom et al.*, 1997, 1998] (Figure 6). The overall importance of flooding is discussed in section 3.2.

Where the snow is damp/wet with a low water content, which is often the case close to the snow/ice interface, clusters of rounded crystals form, held together by large ice-to-ice bonds [*Colbeck*, 1986]. Subsequent freezing leads to rounded melt-freeze particles, whereby individual crystals are frozen into a solid polycrystalline grain; this produces a coarse-grained snow. In summer, snow is characterized by extensive iciness in the form of icy grain clusters, ice lenses, ice layers, and percolation columns as a result of melt-refreeze cycling, with grain clusters up to 1 cm across [*Haas et al.*, 2001; *Morris and Jeffries*, 2001]. These large clusters may have a strong signature at microwavelengths. In winter, dampened grain clusters are more prevalent toward the snowpack base.

Estimates of mean grain size are presented in Table 5. They range from 1.5 to 2.9 mm and exhibit a considerable spatial and temporal similarity. Figure 7 presents a typical frequency distribution of grain size from snow pit measurements in winter. The mode is 2.0–2.5 mm, and grain size ranges from 0.05 mm for mechanically fragmented spicules of new snow to 10 mm for well-developed depth-hoar cups in older, cold snow. Skeletal depth hoar comprises loose accumulations of cupped and columnar crystals separated by 1–2 mm voids [*Akitaya*, 1974]. *Sturm et al.* [1998] observed that if a given layer

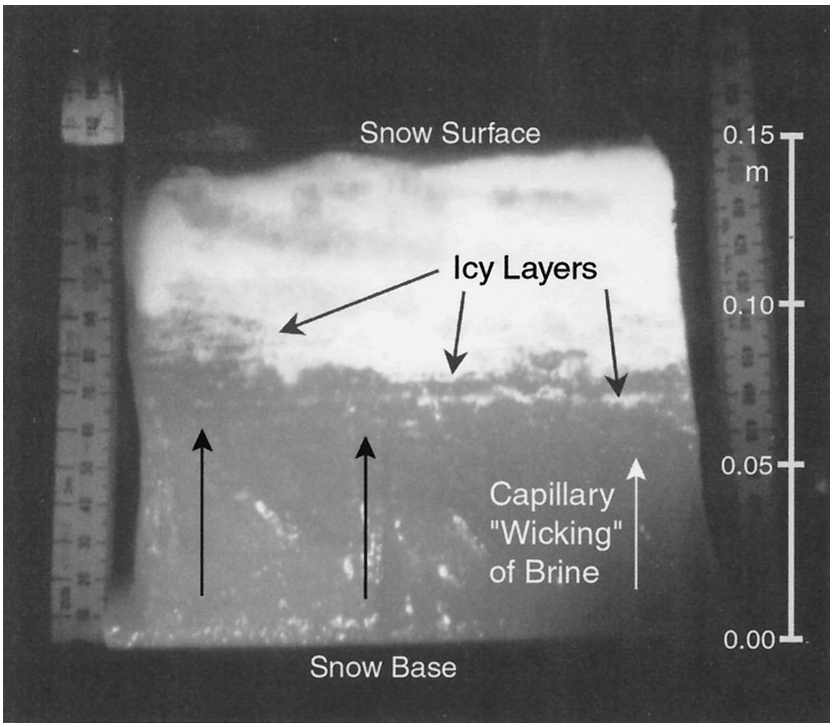

Figure 6. A photograph of dyed seawater percolating, by capillary suction, upward through a block of natural Antarctic snow, removed from winter sea ice (in the Amundsen Sea, September 1994) and transported intact to a cold room. In this experiment, 2 cm of seawater was poured around the snow base. The photograph was taken 30 min later. The whole snow column (14 cm thick) was affected, with the lower 7.5 cm being saturated. Note the lateral spreading out of seawater across icy lenses in the upper part of the snow, which is typically colder.

TABLE 5. Mean Snow Grain Size Measured in Snow Pits, With 1σ

Region	*Season, Year*	*Grain Size, mm*	*Range, mm*	*n*[a]	*Reference*
		Indian and Western Pacific Oceans			
75°–150°E	spring 1994	1.7 ± 0.8	0.05–4.00	17	*Worby and Massom* [1995]
139°–141°E, 144°–150°E	autumn 1993	1.5 ± 1.5	0.05–10.0	54	*Worby and Massom* [1995]
138°–142°E	winter 1995	1.6 ± 1.2	0.01–10.0	167	*Massom et al.* [1998]
		Bellingshausen, Amundsen, and Ross Seas			
70°–130°W	late summer 1994	2.5 ± 1.0	1.00–4.00	11	*Haas et al.* [2001]
109°–171°W	winter/spring 1994	1.6 ± 0.7	0.80–3.60	49	*Sturm et al.* [1998]
		Weddell Sea			
20°–55°W	late summer 1997	2.9 ± 1.2	0.5–10.0	129	*Haas et al.* [2001]
0°–50°W	winter 1992	2.7 ± 3.1	0.2–10.0	90	*Massom et al.* [1997]

[a]Number of snow samples.

had been subjected to wetting, its grain-size distribution showed a distinct bimodality.

By virtue of its effect on the ratio of absorption to scattering, grain-size growth reduces snow albedo, particularly at near-infrared wavelengths [*Grenfell et al.*, 1994; *Warren*, 1982; *Wiscombe and Warren*, 1980]. Moreover, grain enlargement can increase the intensity of shortwave radiation penetration by decreasing the spectral extinction coefficient [*Maykut*, 1986]. Similarly, grain-size variability affects the surface electromagnetic signature measured by satellite microwave sensors [*Hallikainen and Winebrenner*, 1992], particularly at higher frequencies [*Comiso*, 1983].

However, more than just a single measure of grain size is needed to understand these effects. For spherical grains, there is no ambiguity. However, for nonspherical grains, the sizes reported here in Figure 7 and Tables 3 and 4 are the longest dimension. This is probably a useful measure for explaining the microwave emissivity, but for snow properties in the solar spectrum, the most relevant dimension is the shortest one (e.g., the width of the column, the thickness of a plate, or the thickness of one wall of a faceted cup. Specifically, the optically effective grain radius is $3V/S$, where V/S is the volume-to-surface ratio [*Grenfell and Warren*, 1999]). This is because the ratio of absorption to scattering is determined by the average distance that photons travel through ice between opportunities for scattering at air-ice interfaces. For example, the depth hoar in Figure 5 may have a grain size as large as 10 mm as determined by sieving, but the optically effective grain diameter appears to be about 0.5 mm. Albedo decreases as grain size increases. This normally results in a decrease of albedo with snow age as destructive metamorphism proceeds. However, growth of depth hoar by constructive metamorphism, although it increases crystal length, does not necessarily increase the average crystal thickness.

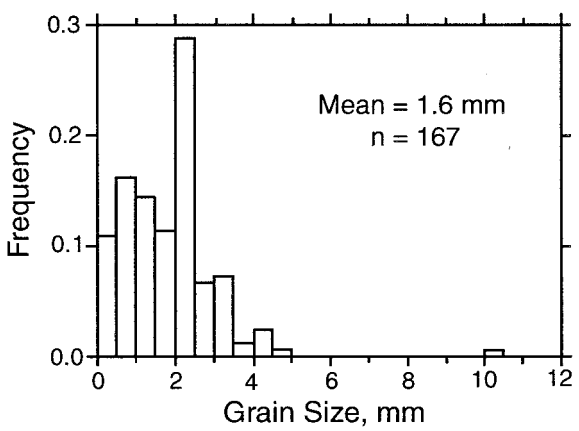

Figure 7. A typical frequency distribution of snow grain size in winter, from East Antarctica. After *Massom et al.* [1998].

2.2.2. Snow density. Snow density affects the effective thermal conductivity (see section 2.2.5) and air permeability and determines the snow-water equivalent and dielectric properties of the snow mass [*Hallikainen and Winebrenner*, 1992]. Large-scale means vary from ~290 to 390 kg m^{-3} (Table 6), similar to values found in the Arctic [*Warren et al.*, 1999, Figure 11]. Density as a function of snow type ranges from 108 kg m^{-3} for new snow to >760 kg m^{-3} for icy layers [*Sturm et al.*, 1998]. Again, great variability occurs on small spatial scales. In East Antarctica in August 1995, for example, average density ranged from 240 to 600 kg m^{-3} across a single floe as determined from 47 measurements at meter intervals [*Massom et al.*, 1998].

Typical wintertime frequency density distributions are shown in Figure 8. The distribution from the Indian Ocean (Figure 8a) shows a mode at 300–350 kg m^{-3}, with a minor peak at ~700 kg m^{-3} comprising icy layers. Lower modal values (225–250 kg m^{-3}) have been reported from the Bellingshausen and Amundsen Seas in the late-winter to early spring [*Jeffries et al.*, 1997b], reflecting the higher proportion of depth hoar present in the older, colder snow cover (see section 2.2.1). The few data collected in summer reveal a high mean density due to melt-refreeze processes [*Haas et al.*, 2001; *Morris and Jeffries*, 2001]. The density of icy samples tends to be

TABLE 6. Snow Densities (Mean and Standard Deviation) Measured Over Antarctic Sea Ice

Region	Season, Year	ρ_s, kg m^{-3}	Range, kg m^{-3}	n[a]	Reference
		Western Pacific Ocean			
139°–141°E, 144°–150°E	autumn 1993	390 ± 170	120–660	55	*Worby and Massom* [1995]
138°–142°E	winter 1995	360 ± 110 414[b]	120–760	170	*Massom et al.* [1998]
		Bellingshausen, Amundsen, and Ross Seas			
95°–165°W	autumn 1992	340 ± 80	99–543	134	*Jeffries et al.* [1994a]
165°–180°E	autumn/winter 1995	350 ± 80	240–817	73	*Sturm et al.* [1998]
75°–110°W	winter/spring 1993	247 ± 210	108–467	210	*Jeffries et al.* [1997a]
109°–171°W	winter/spring 1994	360 ± 40	300–440	255	*Sturm et al.* [1998]
80°–110°W, 155°–180°W	winter/spring 1995	380 ± 80	290–480	45	*Sturm et al.* [1995, 1998]
70°–130°W	late summer 1994	391 ± 71	212–518	37	*Haas et al.* [1996]
		Weddell Sea			
5°E–55°W	autumn/winter 1992	290	200–600	···	V. Lytle (unpublished data, 2001)
0°–50°W	winter 1992	320	180–670	132	*Massom et al.* [1997]
0°–55°W	spring 1989	290 ± 70	110–550	206	*Eicken et al.* [1994]
20°–57°W	late summer 1997	349 ± 72	130–496	130	*Haas et al.* [1998]

[a]Number of snow pits.
[b]Density when adjusted to account for the total proportion of icy layers present.

underestimated due to the difficulty of sample collection for these thin layers.

Generally, snow density can be estimated from the prevailing and recent weather conditions. For dry cold conditions, low-density snow (200–300 kg m^{-3}) predominates; for warm, windy conditions, medium- to high-density snow predominates (350–500 kg m^{-3}); and for melt-refreeze conditions, high-density snow predominates (400–700 kg m^{-3}). Snow overburden is so low that vertical compaction and densification of the seasonal snow cover is likely to be very limited.

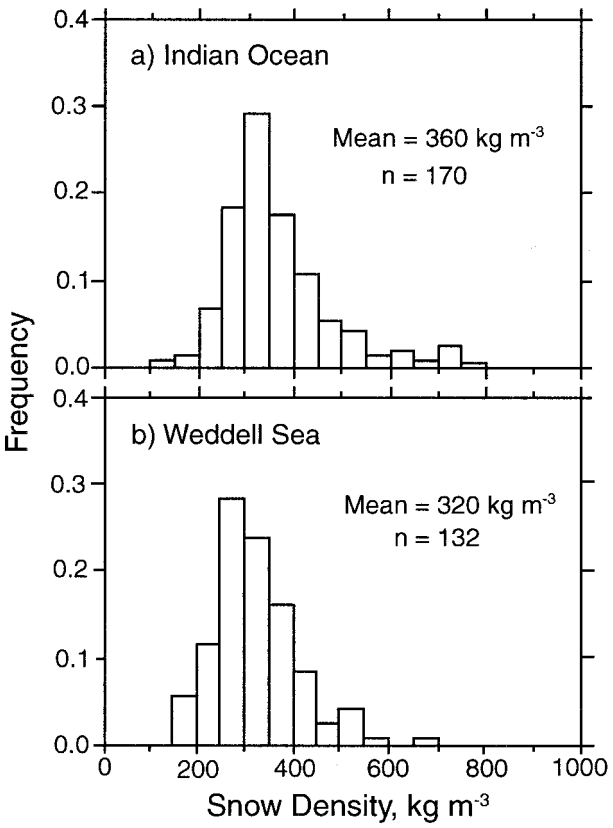

Figure 8. Typical frequency distributions of snow density measured in snow pits from two winter cruises in (a) the Indian Ocean [after *Massom et al.*, 1998] and (b) the Weddell Sea [after *Massom et al.*, 1997].

2.2.3. Snow wetness. Snow wetness or free-water content is typically measured using calorimetry, dilution, and dielectric techniques. *Colbeck et al.* [1990] give a general classification of liquid water content: Snow is said to be dry when the percentage of liquid water is 0%, moist at <3%, wet at 3–8%, very wet at 8–15%, and slush (saturated) at >15%. While few quantitative snow-wetness measurements have been made over Antarctic sea ice, observations suggest that snow wetting due to melt, flooding, and even rainfall (at times) is a key factor, greatly modifying the snow texture, properties, salinity, and optical and microwave characteristics [*Drinkwater*, 1995; *Hallikainen and Winebrenner*, 1992; *Warren*, 1982]. Although melt is most intense in late spring and summer, it occasionally occurs at other times, including winter (section 3.3). Flooding by seawater incursion occurs throughout the year [*Ackley et al.*, 1990; *Eicken et al.*, 1995; *Jeffries et al.*, 1998a; *Takizawa*, 1984; *Wadhams et al.*, 1987; *Worby and Massom*, 1995]. In places, the mass of the relatively thick snow cover (compared with the sea ice) depresses the ice surface below sea level. Seawater infiltration then occurs where cracks or brine-drainage channels interconnect the ocean and ice surface, saturating the basal snow. The resultant slush becomes meteoric ice or "snow ice" on freezing (see section 3.2). Flooding also seeds the snow/ice interface with nutrients and algae, which form productive "infiltration" algal communities [*Ackley and Sullivan*,

TABLE 7. Percentage of Snow Pits and Drilled Holes Containing Slush and Negative Freeboards (z_f) and the Proportion of Snow Ice Measured in Sea-Ice Core Analyses[a]

Region	*Season, Year*	*% Pits With Slush (n)*	*% $z_f \leq 0$ m (n)*	*Mean z_s/z_i*	*% Snow Ice*	*Reference*
			Indian and Western Pacific Oceans			
136°–138°E, 63°–65°S	early spring 1991	···	···	0.37 (7)	30	*Worby and Massom* [1995]
64°–106°E, 59°–69°S	late spring 1991	···	···	0.10 (39)	18	*Worby and Massom* [1995]
62°–102°E, 60°–69°S	spring 1992	···	39 (23)	0.07 (67)	23	*Worby and Massom* [1995]
75°–150°E, 59°–69°S	spring 1994	40 (10)	35 (54)	0.18 (106)	···	*Worby and Massom* [1995]
139°–150°E, 64°–66°S	autumn 1993	53 (17)	11 (134)	0.09 (186)	9	*Worby and Massom* [1995]
138°–142°E	winter 1995	29 (46)	18 (577)	0.19 (584)	···	*Massom et al*. [1998]
			Bellingshausen, Amundsen, and Ross Seas			
165°–180°W	autumn/winter 1995	36 (73)	29 (3671)	0.21/0.31	25 (15/38)[b]	*Jeffries and Adolphs* [1997]; *Sturm et al*. [1998]; *Jeffries et al*. [1998b]
175°E–175°W	autumn/winter 1998	0 (43)	17 (3253)	0.18 (3253)	12 (7/25)[b]	*Jeffries et al*. [2001]; *Morris and Jeffries* [2001]
80°–110°W, 155°–180°W	winter/spring 1995	51 (45)	34 (4025)	0.32 (4176)	?	*Sturm et al*. [1998]
75°–110°W	winter/spring 1993	35	18	0.29	24	*Jeffries et al*. [1997b]
109°–171°W	winter/spring 1994	46 (165)	51 (2227)	0.35	38	*Sturm et al*. [1998]; *Jeffries et al*. [1998a]
70°–130°W	late summer 1994	12 (170)	17 (170)	···		*Haas et al*. [1996]
			Weddell Sea			
0°–55°W	winter/spring 1989	50	40	0.27 (5339)	8	*Ackley et al*. [1990]; *Lange et al*. [1990]
7°E–5°W, 56°–70°S	winter 1986	···	17	0.18 (4238)	···	*Wadhams et al*. [1987]
0°–50°W	winter 1992	···	11.5 (468)	0.14 (386)	···	*Massom et al*. [1997]
46°–54°W, 59°–64°S	spring 1988	···	15	0.23 (1553)	···	*Eicken et al*. [1994]
45°–55°W	summer 1992	30–50 (~100 holes)	···	···	···	*Drinkwater and Lytle* [1997]

[a] *Eicken et al*. [1994] estimated that snow contributed ~8% to the total sea-ice mass in the Weddell Sea, based on results from several field experiments. Numbers of measurements (pits and/or holes) are in parentheses. The ratio of snow to ice thickness is also given.
[b] The first figure is for the inner pack, and the second is for the outer pack (see text).

1994]. The effect of this snow overburden is a fundamental difference between the two polar regions; such flooding is common in the Antarctic but rare in the Arctic (although it may play a significant role in marginal seas such as the Greenland Sea).

Table 7 shows how frequently negative ice freeboard (z_f) was observed on different cruises; this varies from 11 to 51%, and is paralleled in the percentage of slush occurrence. Freeboard is typically close to zero [*Jeffries et al*., 1998b], possibly due to cycles of snow-ice formation, implying that little additional accumulation is necessary to submerge the snow/ice interface and cause flooding [*Eicken et al*., 1994]. *Sturm et al*. [1998] suggest that there is a "self-balancing" mechanism in snow-ice formation, whereby if a negative freeboard is observed, it has to be a short-lived phenomenon in most cases, as snow-ice will form shortly thereafter, reasserting the balance and producing a zero freeboard.

Other processes are responsible for flooding, as depicted in Figure 9. In the outer pack, or marginal ice zone, wave-ice interaction can fragment existing floes and can tilt smaller floes to introduce seawater onto their surfaces, removing much of the snow cover. Saline ponds, caused by the fracturing of, and rubble buildup on, small floes and subsequent wave overwashing or flooding, are a common feature of the marginal ice zone at all times of year [*Ackley and Sullivan*, 1994; *Massom et al*., 1997, 1998; *Wadhams et al*., 1987]. These "deformation ponds" (Figure 9b), which are not to be confused with freshwater melt ponds, cover up to 20–30% of the surface in places and occur up to 200 km in from the ice edge [*Massom et al*., 1998]. In lowering the surface albedo, these processes may play a significant role in enhancing the rapid meltback of the Antarctic seasonal sea-ice zone during the austral spring-summer period.

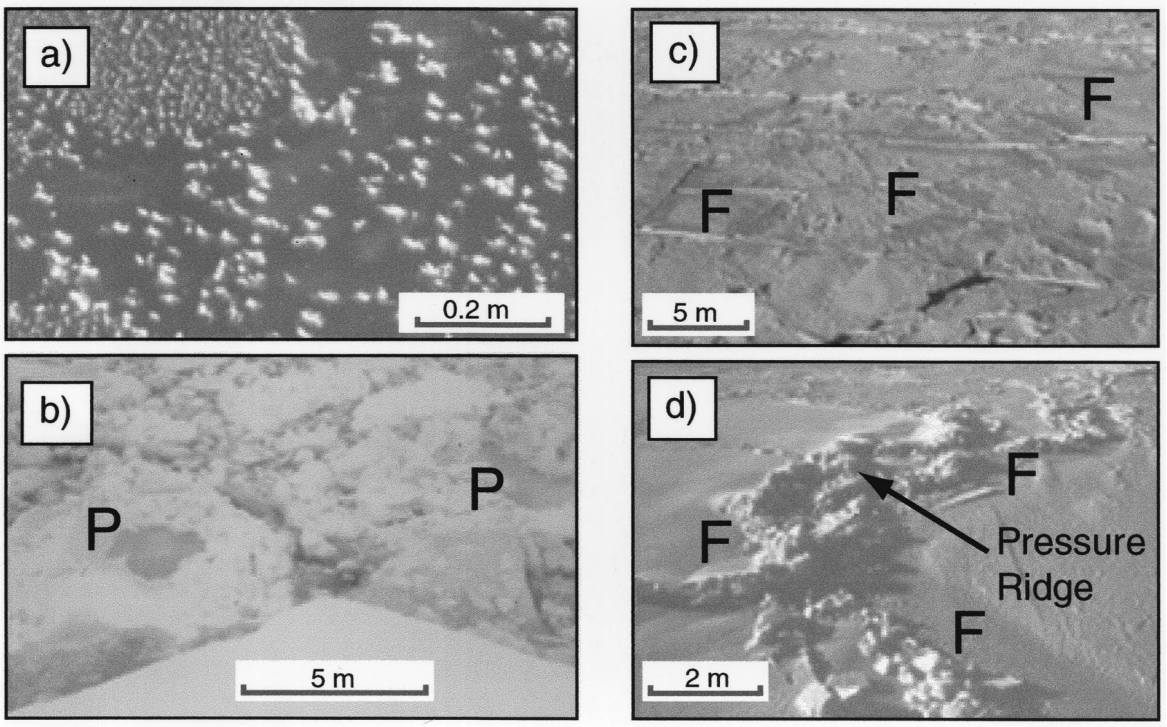

Figure 9. Examples of processes responsible for introducing seawater/high salinity into the snow covering Antarctic sea ice: (a) frost flowers; (b) deformation ponding; (c) wave-induced ice cracking and squirting; and (d) ice depression adjacent to pressure ridges. Letter F denotes regions of flooding, and P denotes ponding. Ridged floes may at times have less flooding (and less snow-ice formation), due to the increased buoyancy of the ice mass contained in the ridges [*Jeffries et al*., 1998a].

Periodically, long-period swell penetrates deeply into the pack and floods the surface of the interior sea-ice zone [*Morris et al*., 1998; *Squire et al*., 1986]. *Worby et al*. [1996a] observed the breakup of ice by swell 300 km south of the East Antarctic ice edge in winter. As the swell propagated through the pack, linear fractures opened on the crest before closing on the trough a few seconds later, leading to the "squirting" of seawater onto the floe surface, as shown in Figure 9c. This process flooded an estimated 20% of the surface over a meridional band ~75 km wide [*Massom et al*., 1999] and caused a distinct greying of the surface. Although the frequency of such events is unknown, it is likely that they periodically add salt and water to the snow. Such processes significantly alter both passive [*Massom et al*., 1999] and active [*Remund et al*., 2000] microwave signatures from satellite remote sensing.

Even in the absence of flooding, the basal snow layer tends to be moist or wet [*Massom et al*., 1998], due to wicking of brine upward through the snow cover. *Steffen and DeMaria* [1996] observed that brine in snow remains liquid to temperatures as low as −15°C. Brine expulsion onto the ice surface occurs during the initial stages of ice formation [*Perovich and Richter-Menge*, 1994] and also occasionally throughout the lifetime of a floe as warming intermittently increases the ice porosity [*Tucker et al*., 1992]. *Garrity* [1992] measured a wetness of 2% just above the slush layer in the Weddell Sea in winter and reported that for air temperatures between −5° and 0°C, significant free water is often present in the snow cover, to a maximum of 2% just above the snow/ice interface. *Mätzler et al*. [1982] showed that snow wetness greater than 1% has a significant effect on the microwave emissivity.

2.2.4. Snow salinity. As a result of the above processes, snow on Antarctic sea ice outside the summer melt period is typically saline [*Massom et al*., 1997, 1998]. Mean snow salinities, measured from the electrical conductivity of melted snow samples, are presented in Table 8. While ranges are large, bulk values from three East Antarctic cruises are strikingly similar to those obtained from the Weddell, Bellingshausen, Amundsen, and Ross Seas in winter. In all cases, salinities cover a wide range of values (0.1–91.8 practical salinity units (psu)). A typical frequency distribution is presented in Figure 10. On many of the voyages, particularly in the Indian and western Pacific Ocean regions, no salt-free snow was found.

As a result of capillary suction of brine, high salinities (>10 psu) occur up to about 0.1 m in the snow column, but mainly in the 0.00–0.05 m layer [*Massom et al*., 1997, 1998], as shown in Figure 11. Mean salinities of the basal snow layer (0.00–0.03 m above the sea-ice surface) are presented in Table 9 and are consistently high in autumn-spring, ranging from 15 to 24 psu. However, there is again a high degree of horizontal variability on small

TABLE 8. Volume-Integrated Average Snow Salinities From Various Antarctic Sea-Ice Experiments

Region	*Season, Year*	*Snow Salinity, psu*	*Range, psu*	*n*	*Reference*
		Indian and West Pacific Oceans			
75°–150°E	spring, 1994	8.8 ± 13.3	0.1–66.4	41	*Worby and Massom* [1995]
139°–141°E, 144°–150°E	autumn, 1993	8.4 ± 13.5	0.1–47.1	51	*Worby and Massom* [1995]
138°–142°E	winter, 1995	8.5 ± 10.6	0.1–54.5	202	*Massom et al.* [1998]
		Bellingshausen, Amundsen, and Ross Seas			
75°–110°W	autumn/winter, 1993	8.7 ± 10.6	0.02–36.3	84	*Jeffries et al.* [1997a]
165°–180°W	autumn/winter, 1995	8.7 ± 10.2	0.02–39.8	193	*Jeffries and Morris* [2001]
175°E–175°W	autumn/winter, 1998	13.1 ± 18.5	0.01–91.8	179	*Jeffries and Morris* [2001]
109°–171°W	winter/spring, 1994	2.6 ± 6.5	0.01–40.5	333	*Jeffries et al.* [1997b]; *Sturm et al.* [1998]
70°N–130°W	late summer, 1994	0.02 ± 0.08	0.00–0.36	37	*Haas et al.* [1996]
		Weddell Sea			
0°–55°W	spring, 1989	4.0	0.0–41.9	87	*Eicken et al.* [1994]
20°–55°W	late summer, 1997	0.15 ± 0.8	0.0–8.6	130	*Haas et al.* [1998]
5°E–55°W	autumn/winter, 1992	2.6	···	···	*Lytle and Ackley* [1992]
0°–50°W	winter, 1992	8.7 ± 10.7	0.0–48.8	189	*Massom et al.* [1997]

scales, with *Massom et al.* [1998] reporting values ranging from 4.7 to 34.8 psu along one transect across a smooth, unridged first-year floe.

Particularly high basal salinities (>34 psu) can occur due to the incorporation of "frost flowers" (Figure 9a) into the accumulating snow mass [*Massom et al.*, 1997]. Frost flowers form dense mats, a few centimeters thick, on snow-free new ice (nilas) by ice deposited directly on the surface from the vapor phase [*Tucker et al.*, 1992] and attain salinities as high as 110 psu [*Drinkwater and Crocker*, 1988] as they absorb concentrated brine from the ice surface by capillary suction. They are a strong source of radar backscatter, because they form a highly saline, rough dielectric interface compared with smooth sea ice [*Drinkwater and Crocker*, 1988]. Further concentration of brine may occur in the snow mass by sublimation, and with colder temperatures as more solid ice forms (and also crystallization of the different constituent salts at lower temperatures) [*Anderson*, 1960]. Such processes raise the snow melting point, particularly in its lower layers.

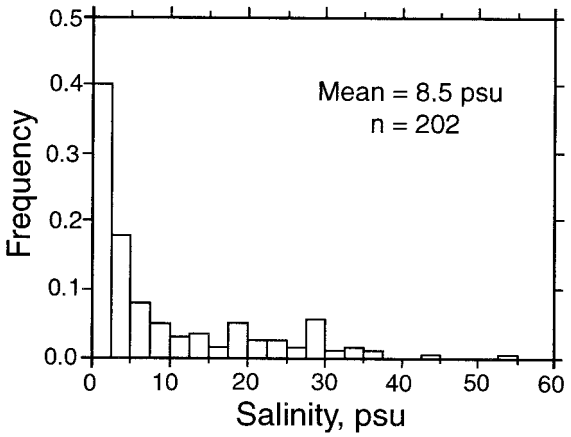

Figure 10. A frequency distribution of snow salinity from the Indian Ocean, August 1995. Typical frequency distributions (outside summer) are weakly bimodal, with a dominant low-salinity peak tailing off to secondary peaks at 20.0–30.0 psu, corresponding to slush and dampened basal snow. After *Massom et al.* [1998].

The low "background" salinity of <1 psu above a height of about 0.3 m in Figure 11 is due to the input of aerosol salts or sea spray from above, or the incorporation of snow that has acquired salt while blowing across the surface of bare ice. Blowing snow collected just above the surface has salinities ranging from 0.1 to 2.0 psu [*Massom et al.*, 1998]. The few data collected during summer [*Haas et al.*, 2001; *Morris and Jeffries*, 2001] indicate low snow salinities of <1.0 psu (Table 8), probably as a result of desalination by percolating snow meltwater.

2.2.5. Effective thermal conductivity of snow. Calculations of conductive heat flux through the snow, which are essential in the modeling of sea-ice growth and decay, depend not only on ∇T but also on the chosen value of the snow thermal conductivity. The latter is defined as the proportionality constant between ∇T and the total heat transport across the snow and is generally expressed as "effective" thermal conductivity to account for all of the processes in the snowpack, including conduction and vapor diffusion, but without airflow [*Sturm and Johnson*, 1992; *Yen*, 1981].

On small scales, the effective thermal conductivity across the layered snow medium is determined not only by the snow temperature but also by its textural characteristics. Various derivations of snow effective thermal conductivity for individual layers containing predominantly one snow type, and defined here as k_{eff}, are reviewed by *Sturm et al.* [1997]. *Sturm et al.* [1998] took direct measurements of k_{eff} for dry snow samples in the Amundsen and Ross Seas using a needle probe appara-

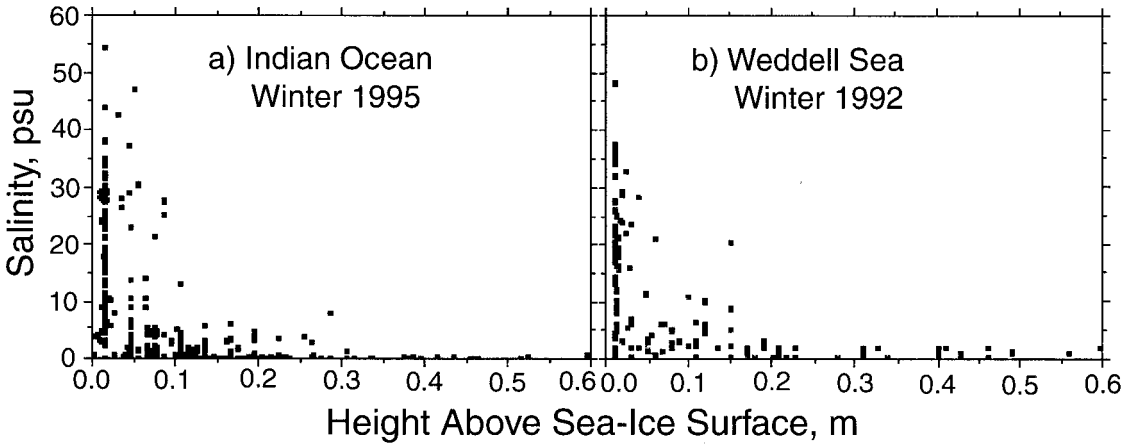

Figure 11. Snow salinity as a function of height in the snow column above the ice surface, for (a) East Antarctica, August 1995 [after *Massom et al*., 1998], and (b) the Weddell Sea, June–July 1992 [after *Massom et al*., 1997].

tus [*Sturm and Johnson*, 1992], with tests designed to preclude thermally driven convection and radiation effects. Analysis of these samples shows that snow on Antarctic sea ice exhibits a wide range of values for k_{eff} (Table 10), depending not only on density (ρ_s) but also on snow microstructure, i.e., grain size, porosity, grain type, and bonding. *Sturm et al*. [1997] concluded that relationships between thermal conductivity and density only occur because (complex) relationships exist between density and microstructure. Although k_{eff} shows a strong density-dependence for snow composed of rounded grains or windblown fragments, there is little density-dependence for snow composed of depth hoar or faceted grains.

Recent work by *Massom et al*. [1998] and *Sturm et al*. [1998] has used this additional detailed information on k_{eff} as a function of snow type (texture) to derive new values for the bulk effective thermal conductivity (k_{bulk}) of snow on Antarctic sea ice. Whereas k_{eff} refers to individual layers of snow, k_{bulk} refers to the sum of the measurements for all of these layers, using the proportions of different snow types observed during entire cruises (e.g., as given in Table 3). Resultant values using data from four field experiments to various sectors of the Antarctic pack are 0.112 (autumn–winter), 0.124 (spring), 0.138 (winter–spring), 0.141 (winter), and 0.164 W m^{-1} K^{-1} (winter). These values are significantly lower than those typically assumed in models, for example, ~0.31 W m^{-1} K^{-1} given by *Hibler* [1979] and *Maykut* [1986]. Other workers [e.g., *Jordan*, 1991; *Yen*, 1981] calculate snow k_{bulk} as a function of density. For comparison, *Brandt and Warren* [1997] measured k_{eff} values of ~0.18–0.35 W m^{-1} K^{-1} for continental Antarctic snow, with k_{bulk} increasing with depth. They suggest that the lower values are associated with a newer snow cover that is significantly less sintered (i.e., has less intergrain bonding) than the compacted layers at depth.

The discrepancy between measured values and those typically used in models also highlights the great difference in the scales involved, i.e., the small scale of measurements (basically hand-specimen size) versus the much larger scale of the model domain (tens to hun-

TABLE 9. Mean Salinities of the Basal Snow Layer (0.00–0.03 m Above the Sea-Ice Surface)

Region	*Season, Year*	*Salinity, psu*	*Range, psu*	*n*	*Reference*
		Western Pacific Ocean			
139°–141°E, 144°–150°E	autumn 1993	23.7	1.8–46.5	11	*Worby and Massom* [1995]
138°–142°E	winter 1995	17.0	0.1–54.4	76	*Massom et al*. [1998]
		Bellingshausen, *Amundsen*, and Ross Seas			
165°–180°W	autumn/winter 1995	20.7 ± 10.8	0.1–49.0	61	*Sturm et al*. [1998]
165°–180°W	autumn/winter 1995	15.8 ± 14.3[a]	0.1–39.1	80	*Jeffries and Morris* [2001]
175°E–175°W	autumn/winter 1998	22.4 ± 20.8[a]	0.7–91.8	93	*Jeffries and Morris* [2001]
109°–171°W	winter/spring 1994	13.3 ± 8.0	1.0–41.0	18	*Sturm et al*. [1998]
80°–110°W, 155°–180°W	winter/spring 1995	16.6 ± 10.9	0.0–47.0	47	*Sturm et al*. [1998]
75°–110°W	winter/spring 1993	15.7	2.0–29.4	34	*Jeffries et al*. [1994a]
		Weddell Sea			
0°–50°W	winter 1992	16.2	0.5–47.8	55	*Massom et al*. [1997]

[a]Measurements taken 0–0.05 m above the sea-ice surface.

TABLE 10. Average Effective Thermal Conductivities of Snow Types, Including 173 Antarctic Measurements Made by *Sturm et al.* [1998][a]

Snow Type	*ICSG Class*[b]	*n*	*Snow Density, kg m^{-3}*	k_{eff}, *W m^{-1} K^{-1}*	*Range in k_{eff}, W m^{-1} K^{-1}*
New snow	1a–1e	10	133 ± 53	0.070	0.039–0.117
Recent snow	2a, 2b	21	254 ± 68	0.128	0.056–0.200
Small rounded grains	3a	51	320 ± 81	0.169	0.051–0.632
Larger rounded grains	3b	9	345 ± 36	0.163	0.083–0.278
Mixed forms	3c, 4c	26	321 ± 29	0.153	0.099–0.218
Depth hoar in chains, weak	5b	171	225 ± 55	0.072	0.021–0.142
Depth hoar, indurated	5a–5c	9	345 ± 73	0.183	0.062–0.330
Clustered rounded grains	6a	1	290	0.188	···
Refrozen wet polygrains	6b	20	422 ± 58	0.250	0.095–0.445
Soft to moderate wind slab	3a, 9d	50	348 ± 33	0.167	0.061–0.281
Hard wind slab	3a, 9d	16	379 ± 45	0.237	0.141–0.316
Hard drift snow	3a, 9d	77	440 ± 34	0.355	0.150–0.541
Very hard wind slab	3a, 9d	22	488 ± 50	0.452	0.240–0.654

[a]Ranges and average snow densities are also given. See also *Sturm et al.* [1997]. The thermal conductivity of sea ice approximates 2.20 W m^{-1} K^{-1} [*Untersteiner*, 1961]. After *Sturm et al.* [1998].
[b]*Colbeck et al.* [1990].

dreds of kilometers). The term k_{eff} when used on the different scales has a complex and wide range of physical meanings, which are beyond the scope of this paper, but is likely to be responsible for some if not all of the mismatch in values.

2.2.6. Albedo of Antarctic sea ice. Sunlight is scattered by bubbles and brine pockets in sea ice [*Grenfell*, 1983]. The albedo of bare sea ice is determined mainly by its thickness, with albedo increasing with thickness [*Perovich*, 1998]. However, in the Antarctic, the sea ice usually acquires a snow cover within a few days after it forms. Thereafter its albedo is determined almost entirely by the snow properties, primarily the snow depth but also the grain size and wetness [*Brandt et al.*, 1999]. In the Ross Sea, for example, *Zhou et al.* [2001] found that the total albedo of the snow on sea ice decreased between the continent and the ice edge, i.e., from south to north, due to an increase in snow wetness and grain size.

Measurements were made on two East Antarctic voyages (in October–November, 1988 and 1996) of the spectral and broadband solar irradiance incident on, and reflected by, the various types of ice encountered in springtime, using a spectral radiometer covering the wavelength range 320–1060 nm with 11 filters and a broadband pyranometer (0.3–2.8 μm). Most measurements were made within 2 hours of solar noon in order to experience the maximum solar altitude. Surface types sampled were water, grease ice, pancakes, nilas, snow-covered nilas, snow-free first-year ice, and snow-covered first-year ice.

The results of broadband solar albedos, covering the wavelength range 0.3–2.8 μm, are summarized in Table 11. This is an updated version of the table published by *Allison et al.* [1993], which had been based on the 1988 experiment only. The most important difference is that the albedos in the "thin snow" category are higher than the estimates given in the 1993 table. The dramatic rise in albedo caused by adding a thin snow layer, of only a few millimeters, to thick sea ice is discussed and explained by *Warren et al.* [1997].

3. THE IMPORTANCE OF SNOW ON ANTARCTIC SEA ICE

3.1. Snow Thickness Distribution

3.1.1. Small-scale variability. On decameter scales, significant thickening occurs on rough (ridged) ice through the formation of sastrugi [*Massom et al.*, 1997, 1998]. Formed when wind speeds exceed ~7 m s^{-1} [*Gow*, 1965], sastrugi (Figure 12a) contain snow 2–5 times thicker than on adjacent, wind-scoured ice [*Eicken*

TABLE 11. Broadband Solar Albedos for Cold Antarctic Sea-Ice Types, From *Brandt et al.* [1999][a]

Ice Type	*Snow-Free*	*Thin Snow, Continuous, <3 cm*	*Thick Snow, ≥3 cm*
Open water	0.07	···	···
Grease ice	0.09	···	···
Nilas, <0.1 m	0.16[b]	0.42	···
Young grey ice, 0.1–0.15 m	0.25	(0.52)	(0.70)
Young grey-white ice, 0.15–0.30 m	(0.35)	(0.62)	(0.74)
First-year ice, 0.3–0.7 m	(0.42)	(0.72)	0.77
First-year ice, >0.7 m	0.49	0.81	0.85

[a]Values in parentheses are interpolated or extrapolated, not measured. Ice with patchy snow cover has an albedo intermediate between snow-free ice and ice with thin snow cover, weighted by the fractional area of snow patches.
[b]Nilas albedo varies with ice thickness from 0.07 to 0.25; 0.16 is the middle of the range.

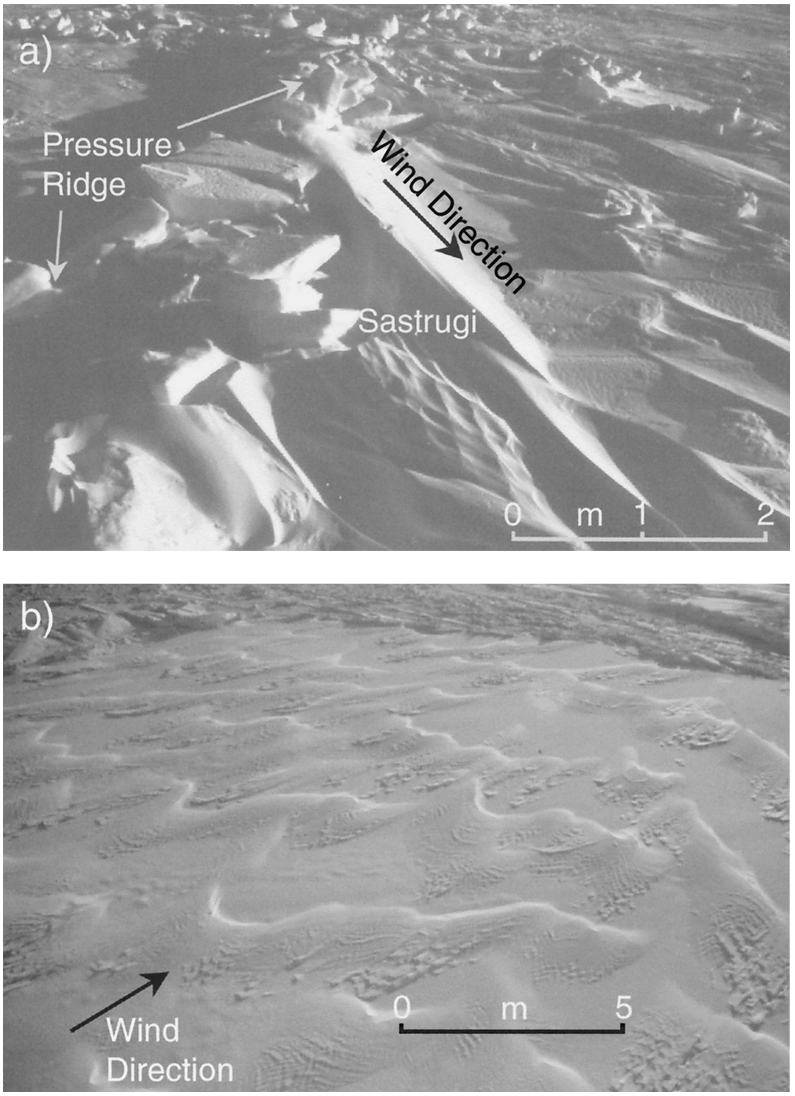

Figure 12. Significant localized snow thickening occurs in the form of (a) sastrugi forming in the lee of surface roughness features such as pressure ridges, and (b) barchan dunes, Indian Ocean in August 1995. Note the cross bedding in Figure 12a, due to floe rotation and changes in prevailing wind direction.

et al., 1995; *Massom et al*., 1997] and can affect more than 50% of the surface area of ridged floes [*Massom et al*., 1998]. On large flatter floes where the areal extent of ridging is less than 5%, low barchan dunes dominate (Figure 12b). Typically covering 40–50% of the surface, these dunes increase snow thickness (z_s) by a factor of 1.5–3 [*Massom et al*., 1997, 1998]. Such thickening can significantly affect the isostasy of newly refrozen lead ice [*Massom et al*., 1998]. Decimeter-scale point aerodynamic roughness features, such as weathered clumps of surface hoarfrost crystals (initially formed under clear, cold, and calm conditions [*Lang et al*., 1984]) or frost flowers, may act as initial foci for low dune formation [*Massom et al*., 1997]. Initially migratory, dunes become semipermanent with time as icy crusts form on their surfaces.

As a result of these processes, z_s can vary as much across a single floe as it does between floes and different ice types. On the meter to decameter scale, good correlation between snow and ice thickness (z_i) occurs only in regions of new and young ice, as noted in the eastern Weddell Sea by *Massom et al*. [1997] early in the growth season. In general, they found that the correlation between z_s and z_i decreased with increasing z_i. The degree of scatter in the relationship between z_s and z_i increases with the amount of ridging (ice deformation) [*Eicken et al*., 1994].

3.1.2. Snow-surface roughness. Using semivariogram analysis, *Sturm et al*. [1998] reported lengths of snow-surface features in the Bellingshausen, Amundsen, and Ross Seas ranging from 3 to 70 m, with average values of 12.7 m in August–September 1995, 22 m in September–October 1994, and 23.3 m in May–June 1995. This compared with a range of structure lengths for the ice surface of ~4–6 m. The average snow structural amplitude was, at <0.1 m, small, but larger than that of the underlying ice (~0.05 m). Thus the addition of snow increases the topographic relief but tends to

"smooth out" the higher-frequency (i.e., rougher) ice surface. *Sturm et al.* [1998] further concluded that any ice surface roughness feature with a relief >0.2 m "nucleated" a significant snow surface feature. Similar work was carried out in the Weddell Sea by *Andreas et al.* [1993]. In the Ross Sea, *Tin and Jeffries* [2001] found significant correlations between mean snow elevation and mean z_i and between snow-surface roughness and z_i in the Ross Sea.

The aerodynamic smoothing effect of snow tends to reduce the surface drag coefficient of deformed ice [*Andreas et al.*, 1993]; for a given wind speed, the drag coefficient is used to determine the atmospheric stress on the ice surface in order to compute ice motion. *Andreas and Claffey* [1995] and *Andreas* [1995] show the surface drag coefficient to be critically dependent on the alignment of the dominant snowdrift pattern relative to the mean wind direction. Where wind direction is relatively constant, they estimate that the formation of snowdrifts aerodynamically streamlines the surface and can lead to a 30% decrease in drag coefficient in 12 hours. Conversely, a significant shift in wind direction or floe rotation can lead to drift erosion (sastrugi development) and a rapid increase in the drag coefficient before streamlining once again occurs. Sastrugi can also significantly alter the bidirectional reflectance pattern of the surface but cause only a slight reduction in albedo [*Warren et al.*, 1998].

3.1.3. Patterns of large-scale variability. In this section we examine regional and seasonal variability in snow thickness distribution.

3.1.3.1. Regional variability. Snow thicknesses appear to be greatest in the Bellingshausen, Amundsen, and Ross Sea sectors (Table 1), due to higher precipitation rates in these regions (see section 3.5). Moreover, a large contrast in z_s exists between the SE and NW Weddell Sea in winter [*Lange and Eicken*, 1991; *Massom et al.*, 1997] (Figure 13). Thick snow to the west of ~35°W and north of ~65°S occurs in the following western limb of the Weddell Gyre [*Massom*, 1992], which contains a significant proportion of second-year and multiyear ice [*Drinkwater et al.*, 1993]. In the eastern Ross Sea in summer (January–February), z_s increases from west to east [*Morris and Jeffries*, 2001].

A significant thickening of snow (and ice) inward from the ice edge has been noted in East Antarctica [*Allison and Worby*, 1994] and in the Bellingshausen and Amundsen Seas in late winter [*Worby et al.*, 1996b]. The thinner snow cover in the outer pack may be related not so much to lower precipitation rates but rather to other factors such as the removal of the snow cover from older ice by wave and swell action. Moreover, the snow in the outerpack is thinner because it has not had as much time to accumulate compared with the inner pack; that is, the ice in the outer pack is younger.

Work in the western Ross Sea in May–June 1995 [*Jeffries and Adolphs*, 1997] and May–June 1998 [*Morris and Jeffries*, 2001] showed that the thinnest snow (and ice) occurred in a 200-km-wide coastal zone, with the thickest occurring in a continental shelf zone 200–600 km from the coast. In both cases, observed patterns may also result from snow-ice formation, as discussed below (section 3.2).

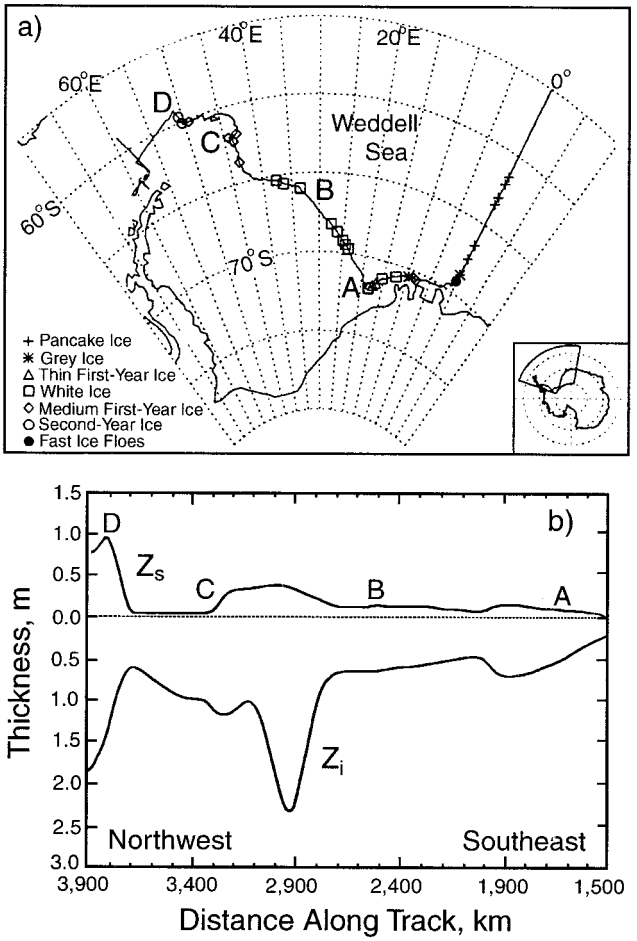

Figure 13. (a) Map showing the cruise track of R/V *Polarstern*, June–August 1992. (b) Mean ice and snow thicknesses from sampling sites along the cruise track, with location indicators A–D as shown in Figure 13a. The curves are interpolated through the mean data points. After *Drinkwater and Haas* [1994].

3.1.3.2. Seasonal variability. Monthly snow-thickness distributions for East Antarctica were presented by *Worby et al.* [1998], based on 10 years of ship-based observations for the months March–April and August–December (Figure 14). The mean snow thickness varies between 0.11 m in March and 0.17 m in both September and December. These data show that in March in East Antarctica, less than 10% of the snow cover is thicker than 0.1 m, with approximately 20% of the pack comprising largely snow-free ice. This is consistent with rapid new ice growth at this time of year. By April, approximately 30% of the snow cover is thicker than 0.1 m, although most of this is in the range 0.1–0.2 m. There is a lower percentage of snow-free ice than in March as the ice cover becomes more consolidated and

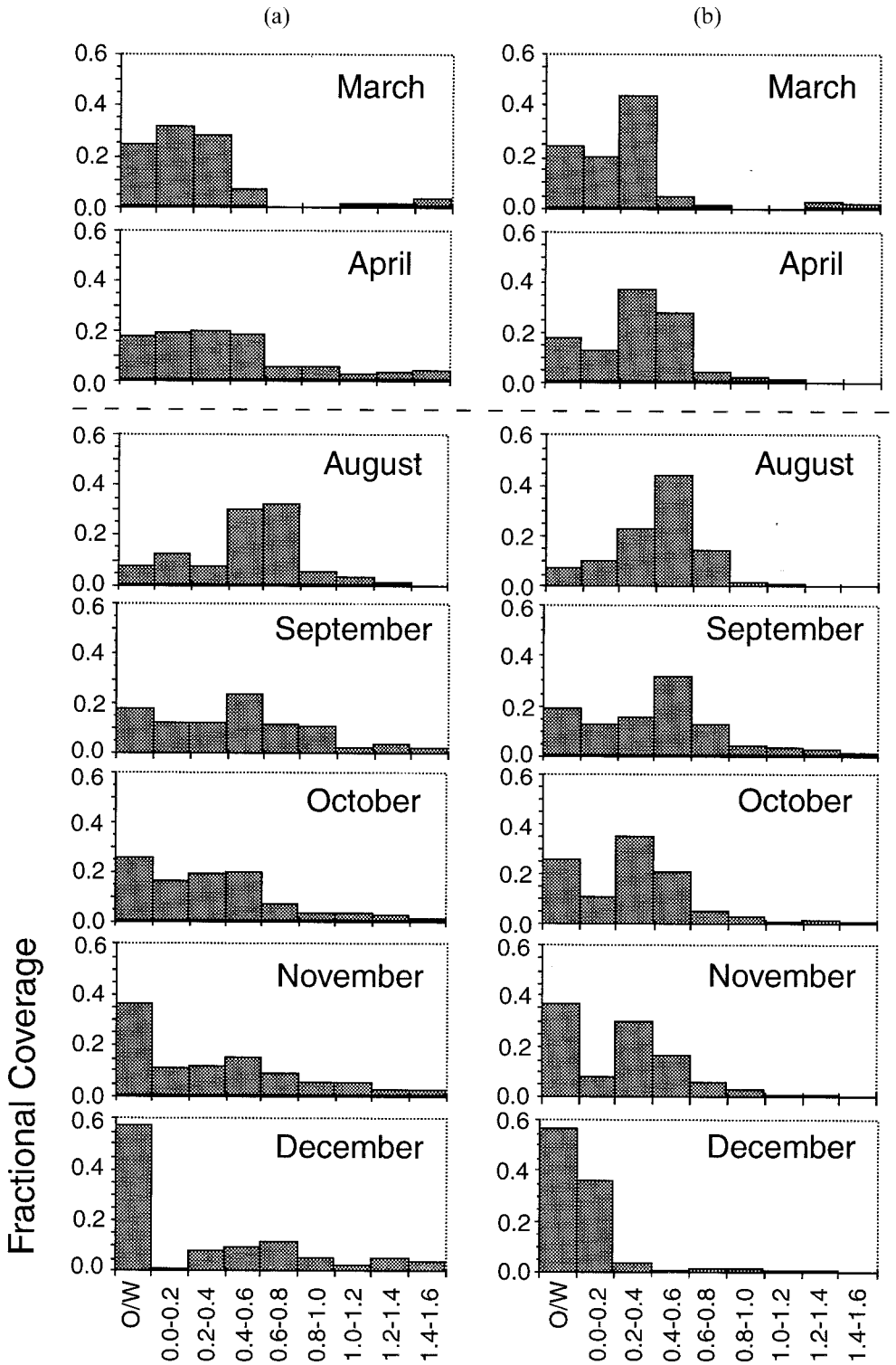

Figure 14. Monthly thickness distributions (in meters) from ship-based observations in East Antarctica for (a) sea ice and (b) snow. The majority of the data have been collected during spring. From *Worby et al*. [1998].

begins to accumulate a snow cover. By winter (August), there is a strong peak in the 0.1–0.2 m snow thickness category. The fraction of snow-free ice is about 10% and remains fairly constant throughout spring as leads open within the pack and new ice is formed. The changing snow thickness distribution from August to December is characterized by a shift in the modal thickness toward thinner snow categories and a decrease in the coverage of thicker snow. This is partly due to the increase in the fraction of open water within the pack, which is why the monthly-mean snow thickness values are not significantly different throughout the spring. The long tails in

the thickness distribution curves reflect the snow cover on very thick floes, not snowdrifts around ridges, as these were not included in the ship-based observations.

In contrast to the winter, thicker snow is encountered in summer in the SE compared with the NW Weddell Sea (at least in 1997), as shown by *Haas et al*. [2001] and reflected in Table 1. This is likely the result of enhanced melting in the high-latitude northwest rather than of less precipitation. *Haas et al*. [1996] reported snow thicknesses to be lower in the central Bellingshausen Sea than farther south. It is not known whether this results from enhanced melting or whether floes to the north were simply younger (multiyear ice was observed in the Amundsen Sea at the time (February, 1994)). One aspect of melting snow in these regions is that it contributes to the formation of "superimposed ice" rather than simply being removed as meltwater (see section 3.2.2). Another example of relatively thick snow occurrence in summer is described in the eastern Ross Sea [*Morris and Jeffries*, 2001].

3.2. The Contribution of Snow to Sea-Ice Formation

A key role of snow in Antarctic sea ice, and one which sets it apart from snow–sea ice interactions in the Arctic [*Jeffries et al*., 1998a], is the widespread contribution it makes to seawater flooding and the subsequent thermodynamic thickening of the ice from above by snow-ice formation. Snow ice is distinguishable from other forms of granular ice (e.g., frazil ice) by its oxygen isotope signature ($\delta^{18}O$) and to some extent (although not definitively) by its fine-grained structure [*Gow and Epstein*, 1972; *Eicken*, 1998; *Jeffries et al*., 1998b].

While flooding is a widespread phenomenon (section 2.2.4), snow is also incorporated into sea-ice formation by other processes. These include the collapse and refreezing of unconsolidated ridges, rafting of snow-covered floes [*Lange and Hubberten*, 1992], and the freezing of brash ice (sea ice pulverized by wave action in the outer pack). By such mechanisms, it is possible for snow-ice layers to form at any depth within a floe.

Mean regional proportions of snow ice calculated from ice cores vary from 8 to 38% (Table 7). A direct comparison of these results is not possible due to ambiguities in the values presented by different authors, which represent either an average percentage of the composition of individual cores or a percentage of the total length of core sampled [*Jeffries*, 1997]. Most authors are not specific about which value they are presenting; in spite of this, however, it is clear that snow-ice formation is an important process in the formation of Antarctic sea ice and a significant contributor to the total mass budget of the sea ice.

Other interesting findings have emerged from these studies. For example, it has been observed that refreezing of slush and "gap layers" and the formation of snow ice in autumn are responsible for strong convection events within the ice [*Lytle and Ackley*, 1996]. This transports warm seawater into the upper ice layers, producing high net upward heat fluxes and bringing nutrients and biota to the snow/ice interface to support an ice algal bloom [*Fritsen et al*., 1994]. Moreover, *Lytle and Ackley* [2001] suggest that in the Weddell Sea, extensive ice basal melt due to the ocean heat flux [*McPhee et al*., 1996] is largely balanced by continual surface snow-ice growth. Such a mechanism has significant implications for the ocean freshwater budget, as it transports snow vertically downward through the sea ice to melt at the base. Similar processes have been observed in the Pacific Ocean sector by *Jeffries et al*. [2001].

3.2.1. Spatial and seasonal variability in flooding and snow-ice occurrence. Considerable variability has been noted in the seasonal occurrence of flooding and concomitant snow-ice formation. Results shown in Table 7 suggest that snow-ice formation is seasonally dependent, with a lower percentage observed early in the growth season compared with spring [*Worby and Massom*, 1995]. *Sturm et al*. [1998] also note an increase in snow-ice thickness from autumn to winter, corresponding to the increase in snow accumulation; however, the ratio of snow to snow ice was observed to remain nearly constant, due to snow-ice formation. The spatial variability of snow-ice occurrence in the Ross Sea in autumn, when there is a small amount of snow ice in the inner pack ice and 2–4 times as much in the outer pack ice, is similar to the seasonal variability observed elsewhere in the Antarctic pack [*Jeffries et al*., 2001].

Increases in surface flooding observed in summer by *Drinkwater and Lytle* [1997] and *Jeffries et al*. [1998b, 2001] are probably due to basal ice melt by high oceanic heat fluxes. Working in the eastern Ross Sea in summer, *Morris and Jeffries* [2001] further observed a relatively thick snow cover (compared with early winter). Both allow the snow load to depress the ice, and coincide with an increase in ice porosity. Sea-ice porosity and permeability are determined by its liquid-brine volume, which is in turn a function of temperature and salinity [*Cox and Weeks*, 1975]. In the absence of cracking, *Crocker and Wadhams* [1989] suggest that brine drainage channels interconnect between the ocean and ice surface when the ice temperature exceeds −8°C. *Golden et al*. [1998] further suggest that sea ice becomes permeable when its temperature exceeds about −5°C for a salinity of 5 psu, allowing brine carrying heat and nutrients to move through the ice. It can be seen from Table 12 that these temperature thresholds are often exceeded. Numerical simulations of flooding and snow-ice formation indicate that upwelling through fractures is more effective than percolation upward through an interconnected network of brine channels in introducing brine/seawater to the snow/ice interface [*Maksym and Jeffries*, 2000].

Flooding does not always accompany negative freeboards in spring [*Andreas et al*., 1993] and winter [*Massom et al*., 1997, 1998]. When the ice is cold, flooding may be due more to deformation processes (cracking and depression adjacent to ridges, and rafting) than to percolation conduits [*Eicken et al*., 1994]. However, cy-

clical warming events in winter (see Figure 3) cause periodic warming of the ice that is sufficient to induce brine percolation. High-temperature events in winter are discussed in section 3.3.2. Further discussion of brine exchange is given by *Maksym and Jeffries* [2000].

The onset of flooding is characterized by a decrease in the radar scattering signature at high incidence angles during autumn [*Drinkwater et al*., 1998; *Drinkwater and Lytle*, 1997; *Haas*, 2001]. Summer melt and refreeze (superimposed ice formation) results in an increase in area-averaged radar backscatter of 2–5 dB compared with winter values [*Drinkwater and Lytle*, 1997; *Haas*, in press; *Morris et al*., 1998]. These findings are contrary to the decrease in radar backscatter observed in the Arctic summer [*Winebrenner et al*., 1998]. Flooding may also be responsible for masking the passive-microwave signature of Antarctic multiyear ice [*Comiso et al*., 1992].

Significant regional variability has also been observed in the contribution of snow ice to the sea-ice mass balance [*Jeffries et al*., 1998a]. Core analyses by *Ackley et al*. [1990], *Eicken et al*. [1994], and *Lange et al*. [1990] suggest that snow-ice formation makes only a moderate contribution to the sea-ice mass balance in the Weddell Sea. Similar findings have come from East Antarctica [*Worby et al*., 1998], although high percentages of snow ice have been reported at times. In contrast, *Jeffries and Adolphs* [1997] and *Jeffries et al*. [1997a, 1998a, 2001] found that snow ice plays a greater role in the thermodynamic thickening of the ice cover in the eastern and western Pacific sectors than does either frazil or congelation ice. This is attributed to higher precipitation rates in the eastern Pacific sector compared with the Weddell Sea and East Antarctica (as discussed in section 3.5). Latitudinal variability has also been observed in the western Ross Sea [*Jeffries and Adolphs*, 1997; *Jeffries et al*., 2001], with the percentage of snow ice encountered in the outer pack ice region being more than double that in the inner pack ice (Table 7).

Because of the widespread occurrence of snow-ice formation, the snow thickness data described in section 2.1 must underestimate the total snow accumulation prior to the observation time. In the Ross, Amundsen, and Bellingshausen Seas, for example, the snow thickness is often less than the thickness of the snow-ice layers because 45–60% of the snow cover has been entrained in the floes as snow ice [*Sturm et al*., 1998; *Jeffries et al*., 1998b, 2001]. The strong correlation between snow depth and snow-ice layer thickness suggests a means to estimate total snow accumulation from ship-based estimates of snow depth [*Sturm et al*., 1998; *Jeffries et al*., 2001].

While snow-ice formation effectively reduces the thickness of the snow, it also enhances the snow's insulative effect by increasing depth-hoar formation as a result of raising the snow/ice interface temperature and steepening the temperature gradient in winter [*Sturm et al*., 1998]. *Sturm et al*. [1998] suggest that a typical metamorphic change from a moderate slab to depth hoar would decrease the conductive heat flux by a factor of 2 for 0.15-m-thick snow under a similar ∇T. On the other hand, flooding reduces z_s and therefore decreases the snow insulation.

3.2.2. Superimposed ice formation. Snow contributes directly to Antarctic sea-ice thermodynamic growth not only by snow-ice formation but also to a lesser extent by the formation of superimposed ice. By this process, meltwater percolating down through the snow refreezes on contact with the colder ice surface or slush layer to form a layer of ice with a polygonal crystal structure [*Eicken*, 1998; *Haas et al*., in press; *Jeffries et al*., 1994b, 1997a; *Morris and Jeffries*, 2001]. Superimposed ice appears to be a widespread feature of the summer snow cover on perennial ice [*Haas et al*., 2001; *Jeffries et al*., 1994b, 1997a; *Jeffries and Morris*, 2001] and is also associated with fast-ice regions [*Kawamura et al*., 1997]. In the Bellingshausen and Amundsen Seas, *Jeffries et al*. [1997a] reported that superimposed ice comprised 5% of the ice sampled in the region.

Superimposed ice formation has also been observed in winter [*Jeffries et al*., 1997b; *Massom et al*., 1998; *Sturm et al*., 1998; *Worby and Massom*, 1995], once again showing that significant surface melt events occur throughout the year. Although its spatial variability is unknown, it may be more prevalent closer to the marginal ice zone where more melt-freeze cycles occur due to generally warmer air temperatures.

Being rough on the centimeter scale [*Massom et al*., 1998], and owing to its relatively low salinity and the large number of gas bubbles present [*Haas et al*., 2001], superimposed ice potentially contributes to a significant increase in microwave scattering [*Holt and Digby*, 1985; *Onstott and Gogineni*, 1985]. *Haas* [2001] observed a pronounced seasonal cycle in satellite radar backscatter from Antarctic sea ice, with higher values in summer than in winter due to extensive superimposed-ice formation on perennial ice in summer. It may also affect the ice optical and mechanical properties and inhibit the influx of brine from below, as it forms a consolidated, impermeable low-porosity layer on top of otherwise "rotten" sea ice. Superimposed ice formation may also contribute to the "preservation" of the ice cover if it exceeds the rate of bottom melting. That superimposed ice is not associated with the seasonal ice zone in summer may be because it may be flooded soon after formation due to bottom melting.

3.3. Snowmelt Processes

3.3.1. Summer conditions. Melt ponds, which are so characteristic of the Arctic summer, are largely lacking in the south. *Andreas and Ackley* [1982] attributed this to the low relative humidity associated with dry winds draining off the continent, persistently strong winds causing increased latent heat losses from ice to atmosphere, and generally below-freezing air temperatures, which together prevent the elevation of snow

wetness to high levels around Antarctica. As a result, the snow cover remains largely intact, and the surface albedo remains high, in regions retaining ice during summer, i.e., $\sim 4 \times 10^6$ km^2 in February in the western Weddell, Amundsen, Bellingshausen, and eastern Ross Seas [*Gloersen et al*., 1992]. The snow cover itself delays or retards summer ablation from above by restricting the input of solar radiation to melt the ice [*Gow and Tucker*, 1990].

Melt ponds were observed in the NW Weddell Sea and the Amundsen and Bellingshausen Seas in summer (February) 1995; these had a significant effect on the radar backscatter signature of the ice cover [*Drinkwater et al*., 1998; *Drinkwater and Liu*, 2000]. These authors attribute the melt-pond formation to anomalously intense warming events in 1994–1995. Ponds with salinities below those of seawater were also reported from the NW Weddell Sea in January–February 1997 by *Haas et al*. [2001]. Some contained dense algal populations.

Antarctic sea-ice melt occurs primarily from below [*Andreas and Ackley*, 1982; *Gordon*, 1981], as summer air temperatures largely remain below freezing in those areas retaining ice. Surface melt in the Weddell Sea during the onset of summer occurs in patches and is neither spatially nor temporally contiguous at any given time. Ephemeral melt south of the seasonal melt front is due to periodic incursions of warm maritime air, with subsequent returns to cold weather leading to refreezing [*Drinkwater et al*., 1998; *Drinkwater and Liu*, 2000; *Morris et al*., 1998]. The resultant extensive iciness in the snow cover may contribute to the observed increase in radar backscatter in summer [*Haas*, 2001]. In these studies an important distinction is made between seasonal and perennial ice. Covered in thick snow, the latter reacts slowest during brief periods of warming. *Drinkwater and Liu* [2000] conclude that Antarctic sea-ice surface melting is sparse and relatively short lived compared with the protracted summer melt season in the Arctic.

3.3.2. Extensive surface melt in winter. Substantial surface melt periodically occurs at other times of year, even in winter [*Massom et al*., 1997, 1998], as rapidly moving storms transport warm, moist maritime air across the pack [*Andreas*, 1985]. The snow cover, if thick enough, largely protects the underlying ice from melt before freezing conditions return, but undergoes considerable metamorphism resulting in an icier, coarser-grained texture. This sequence recurs a number of times throughout a season [*Massom et al*., 1997, 1998].

Less frequently, and where high temperatures persist, the snow cover may be removed altogether by melt. In the northwestern Weddell Sea in July 1992, an increase in T_{air} from -22°C to 0°C over a 12-hour period (Figure 15a) was accompanied by significant increases in wind speed and relative humidity, with a low, longwave radiation–trapping cloud base (also observed by *Oelke* [1997]). This led to a reversal of the sensible heat flux, melt, and condensation at the surface [*Drinkwater*, 1995], which subsequently refroze to form centimeter-scale icy nodules. Because of prolonged high temperatures (over a 2- to 3-day period) and sleet and even rain, all shallow areas of unconsolidated low-density snow (originally 0.10–0.15 m thick) melted away, leaving a layer of slush on rotting sea ice with a pitted, porous grey surface [*Haas et al*., 1992; *Massom et al*., 1997] but no melt ponds (due to drainage through enlarged brine drainage channels). The effect on radar backscatter is discussed by *Drinkwater et al*. [1995]. The only regions of snow to survive were hardened barchan dunes (Figure 15b). The effect such events have on the salinity and structure of the underlying sea ice and ocean is unknown, although it is likely that the downward flux of freshwater is considerable.

3.4. Snow Thermal Properties and Thermal Environment

3.4.1. Snow temperature. Because of its insulative properties, snow greatly influences the magnitude and direction of heat fluxes and the ice-surface temperature. Snow temperature in turn regulates the composition and salinity of the liquid phase [*Weeks and Ackley*, 1986] and the connectivity of the pore/brine channel pathways in sea ice [*Cox and Weeks*, 1975]. It also plays a central role in the structuring of sea-ice microbial communities [*Eicken*, 1992] and the passive microwave signature of the surface [*Comiso et al*., 1992].

In winter, the snow/ice interface temperature (T_i) is typically significantly warmer than that of the snow surface (T_s), with the snow largely protecting the ice from large variability in T_{air} (Table 12). While T_s is strongly coupled to, and approximates, T_{air} [*Guest and Davidson*, 1994], T_i is highly dependent on z_s and is poorly correlated with T_s.

Seasonal and interannual differences in T_s and T_i translate into significant variability in ∇T [*Sturm et al*., 1998], which affects snow texture through its effect on metamorphism [*Colbeck*, 1982]. Average temperature gradients in winter (shown in Table 12) are typically lower than the critical threshold of about -25°C m^{-1} for depth-hoar growth [*Akitaya*, 1974; *Armstrong*, 1980; *Marbouty*, 1980]. *Sturm et al*. [1998] showed that in the Amundsen, Bellingshausen, and Ross Seas, depth hoar comprised nearly twice as much of the snowpack in autumn than in winter, due to the higher ∇T across a thinner autumn snow cover.

3.4.2. Conductive heat flux through the snow. Using the new lower k_{bulk} value of 0.164 W m^{-1} K^{-1} given in section 2.2.5, *Massom et al*. [1998] examined the temporal variability of the conductive heat flux (F_a) by measuring ∇T over a 16-day period in August 1995 (Figure 16). Rapid and large changes of T_{air} while T_i was much steadier resulted in large heat flux changes through a snow cover that varied in thickness from 0.22 to 0.11 m (due to aeolian erosion). Such temporal variations are similar to near-contemporary spatial varia-

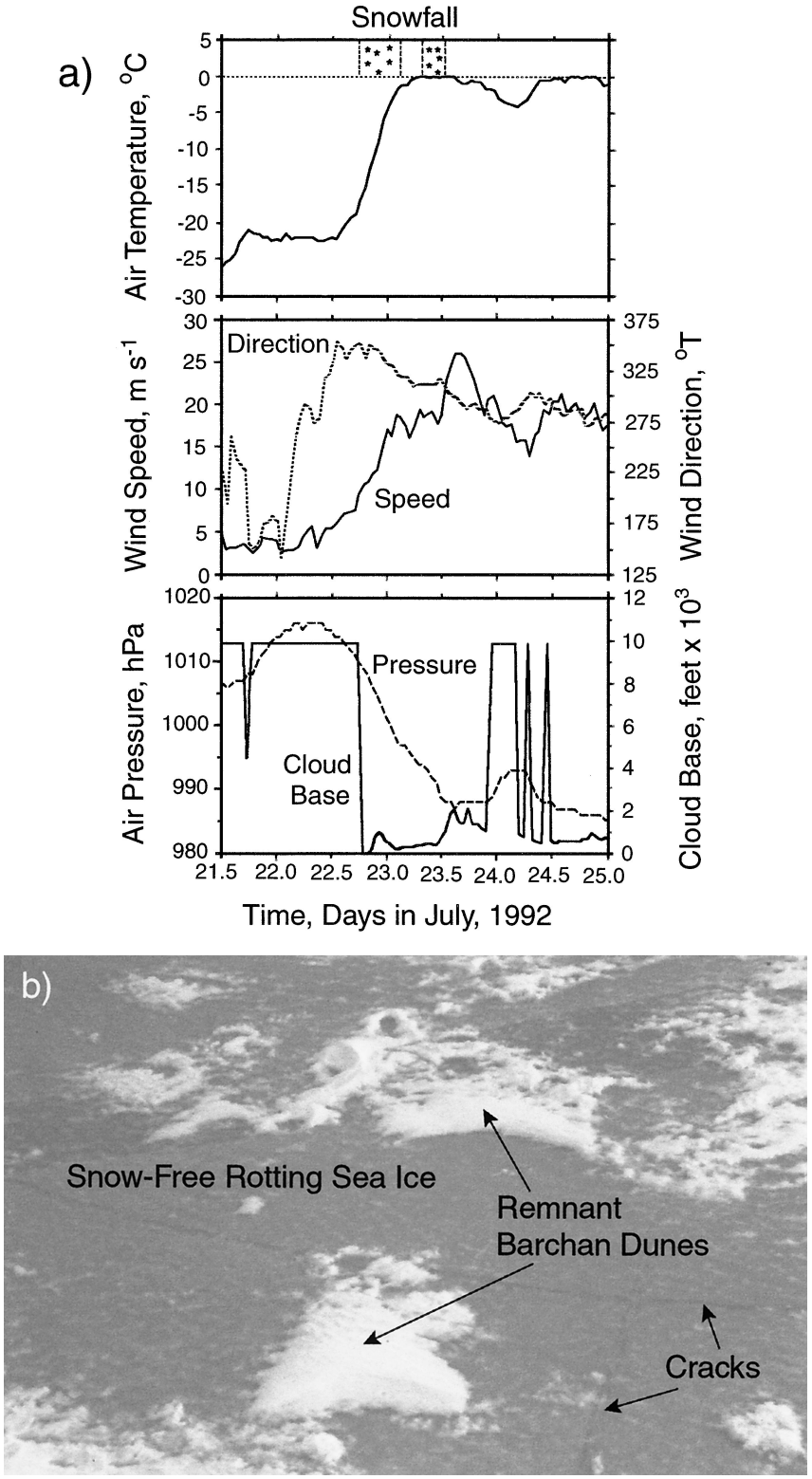

Figure 15. (a) Near-surface meteorological variables measured from R/V *Polarstern* while drifting with the pack ice in the NW Weddell Sea (at ~61°S, 43°W), July 21–25, 1992. After *Massom et al*. [1997]. (b) A photograph, taken on July 25, 1992, showing the effects of the catastrophic snowmelt associated with the significant synoptic-scale temperature increase due to warm air advection, shown in Figure 15a. The surviving barchan dune in the foreground is ~5 m across.

TABLE 12. Mean Values of T_s, T_i, and ∇T (Assuming Linearity) Measured on Antarctic Cruises[a]

Region	*Season, Year*	*Mean T_s, °C*	*Range T_s, °C*	*Mean T_i, °C*	*Range T_i, °C*	*Mean ∇T, °C m^{-1}*	*Range ∇T, °C m^{-1}*	*n*	*Reference[b]*
				Indian and Western Pacific Oceans					
75°–150°E	spring 1994	−5.0	−12.8 to −0.2	−4.9 ± 4.1	−16.0 to −1.9	+10 ± 38	−39 to +104	13	1
139°–150°E	autumn 1993	−11.3	−17.1 to −4.1	−6.1 ± 2.9	−12.5 to −2.1	−66	−229 to +1	16	1
138°–142°E	winter 1995	−13.9	−27.6 to −0.4	−8.7 ± 8.5	−18.7 to −0.8	−47 ± 59	−273 to +79	751	1
				Bellingshausen, Amundsen, and Ross Seas					
165°–180°W	autumn/winter 1995	−18.8	−37.9 to −1.2	−11.8 ± 6.5	−39.9 to −0.1	−82 ± 84	−975 to +208	2986	3
80°–110 and 155°–180°W	winter/spring 1995	−18.1	−29.3 to −0.1	−8.4 ± 3.8	−31.1 to −0.3	−45 ± 39	−562 to +140	2896	2
109°–171°W	winter/spring 1994	−9.8	−24.0 to 0.0	−4.4 ± 2.5	−20.5 to 0.0	−25 ± 41	−570 to +59	2176	2
75°–110°W	winter/spring 1993	−11.6 ± 6.7	−23.2 to −1.0	−5.0 ± 2.3	−13.3 to −2.0	−41 ± 42	−148 to +14	113	3
				Weddell Sea					
0°–55°W	spring 1989	−7.1 ± 5.0	−18.3 to +1.5	−5.8 ± 3.1	−13.0 to −1.0	−10.9 ± 20	−56.2 to +21.4	43	4
0°–50°W	winter 1992	−13.7 ± 8.0	−28.7 to −0.1	−8.0 ± 3.5	−18.0 to −2.4	−47 ± 40	−163 to +0	44	5

[a]In reality, ∇T is seldom linear.
[b]References are 1, *Massom et al.* [1998] and *Worby and Massom* [1995]; 2, *Sturm et al.* [1998]; 3, *Jeffries et al.* [1997b] and M. Jeffries (unpublished data, 2001); 4, *Garrity* [1992]; and 5, *Massom et al.* [1997].

tions observed across single floes as a result of variable z_s [*Massom et al.*, 1998].

Sturm et al. [1998] observed local variations in F_a to be greater in autumn than in winter and concluded that such variability cannot be predicted as a simple function of z_s, as snow stratigraphy does not scale with z_s. On a regional scale they derived mean values for entire cruises ranging from -2.9 ± 5.0 and -6.1 ± 5.3 W m^{-2} in winter to -9.2 ± 9.9 W m^{-2} in autumn. They attribute these differences to the combined effect of seasonal differences in mean values of T_s, k_{bulk}, ∇T, and z_s, as noted earlier.

Recent large-scale modeling studies by *Wu et al.* [1999] imply that the use of correct k_{bulk} values is as crucial to the model performance as the presence of a snow layer and the value of the snowfall rate. They investigated the effects of variations in snow thickness and the magnitude of the thermal conductivity on accretion/ablation in a coupled atmosphere–sea ice model. Using the lower value of 0.164 W m^{-1} K^{-1} [after *Massom et al.*, 1998] instead of 0.31 W m^{-1} K^{-1} changed the modeled sea-ice thickness distribution significantly, with the ice becoming thinner on average by about 0.2 m in the Antarctic (and about 0.4 m in the Arctic). A similar experiment conducted by *Fichefet et al.* [2000] with a global, coupled ocean–sea ice model suggests that changes in the oceanic heat flux at the ice base could reduce this thinning to 0.10 m in the Antarctic.

3.5. Precipitation

Precipitation and accumulation are difficult to measure in situ on sea ice because of strong winds and the formation of snow ice. Variables obtained from atmospheric analysis models may be used to calculate moisture fluxes, with the residual providing an estimate of the net surface moisture balance, the equivalent of precipitation minus evaporation (P-E) or accumulation. This procedure provides a larger spatial and temporal coverage than direct measurements and has been successfully applied to the calculation of snow accumulation over the Antarctic continent [*Budd et al.*, 1995; *Cullather et al.*, 1998]. Owing to the relative coarseness of the data, results obtained from atmospheric parameters are difficult to compare with direct measurements, as the latter are spatially and temporally limited. Moreover, those measurements that do exist often do not represent the total snow accumulation due to snow "loss" when snow ice forms (see section 3.2.1). The magnitude of snow loss directly into the ocean via leads [*Eicken et al.*, 1994] and windblown sublimation [*Déry et al.*, 1998; *Pomeroy and Gray*, 1994] is also largely unknown over sea ice.

A typical accumulation distribution is shown in Figure 17, where 39 months of Global Assimilation and Prediction (GASP) data were used to calculate horizontal moisture fluxes [*Budd et al.*, 1995; *Reid and Budd*, 1995]. Standing waves of cyclonic activity can be seen off the coast of the continent, particularly in the eastern longitudes. Here areas of high accumulation are associated

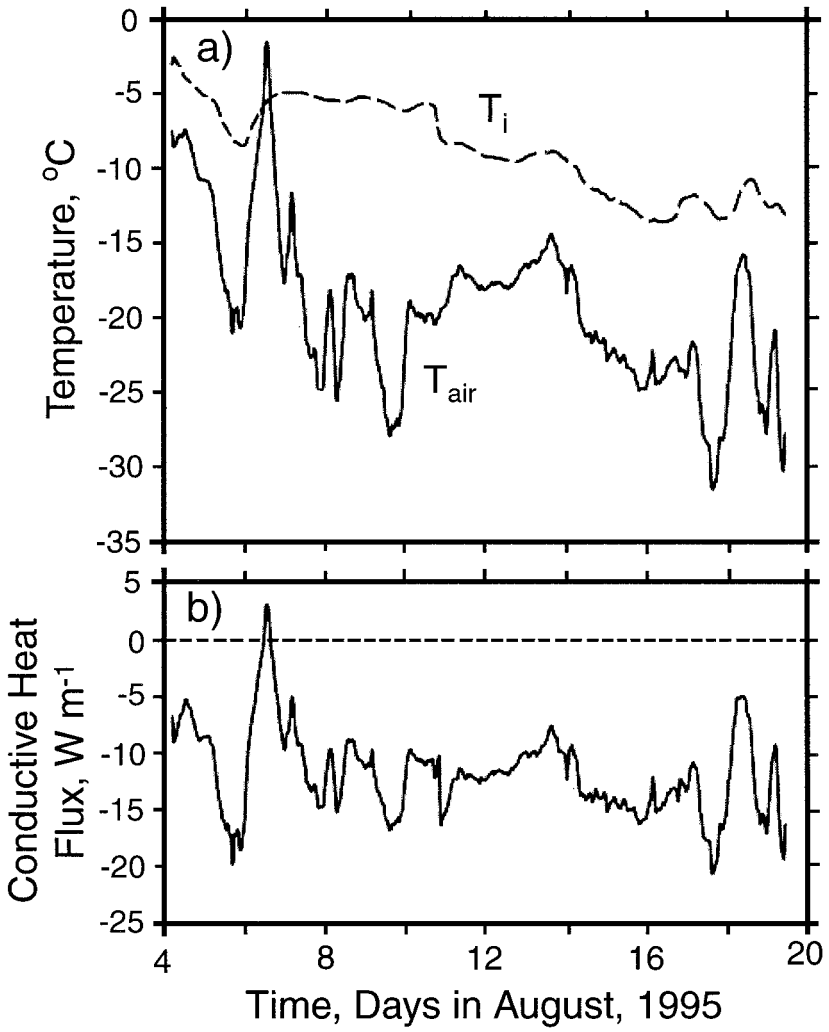

Figure 16. (a) The relationship between T_{air} and T_i derived from hourly thermistor measurements on a single first-year floe. (b) Vertical conductive heat flux in the snow. Negative implies a net conductive heat loss, and positive implies a net gain. After *Massom et al*. [1998].

with air masses flowing south toward the coast, with outflow producing drier conditions. Figure 18 shows the annual cycle of zonal mean net accumulation for several latitudes north of the Antarctic coast. A well-defined annual cycle is shown, with maximum values of accumulation occurring in July through September and a distinct minimum occurring during December. While the maximum snow accumulation around the zone is shown to be about 44 mm per year (during July), accumulation rates vary quite considerably within the zone (Figure 17).

3.6. Implications of Global Warming

Global climate models [e.g., *Hunt et al*., 1995] predict increased precipitation over the Antarctic sea-ice zone. The implications, and feedbacks involved, are complex. Using a global coupled atmosphere-ocean sea-ice model, *Wu et al*. [1999] showed that changes in snowfall related to global climate change have opposite effects in the Arctic and Antarctic sea-ice regions. When either snow is removed or the snowfall rate is doubled, ice becomes thicker in winter over most of the Antarctic sea-ice zone (Figure 19). For "no-snow," the decrease in thermal insulation causes increased ice growth at the base of the ice. A doubling of the snowfall results in an increase in ice thickness by increased snow-ice formation, which counterbalances the increase in insulation afforded by the thicker snow. By contrast, both no-snow and double-snow conditions result in an apparent thinning of ice in the Arctic. These differences are due primarily to the relative differences in z_i and z_s between the two polar regions.

Eicken et al. [1995] further suggested that the decrease in conductive heat flux under a thicker snow cover would enhance the sensitivity of basal thermodynamic ice growth to oceanic heat flux while decreasing the ice surface sensitivity. Of course, dynamic processes such as ridging and rafting would continue to thicken sea ice [*Worby et al*., 1998].

Figure 20 is a schematic of possible effects on Antarctic air-sea-ice interactions and biota of increased pre-

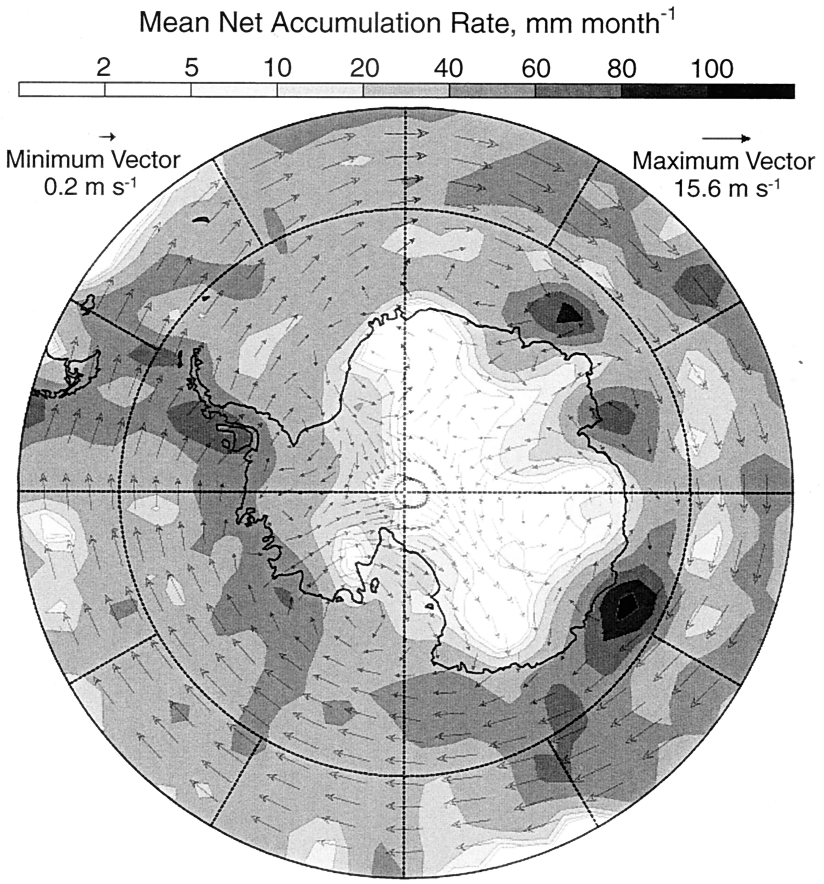

Figure 17. Map of the mean net accumulation rate (mm month^{-1}) from Global Assimilation and Prediction (GASP) data (for the period September 1989 to November 1992), with the reduced-grid yearly mean surface wind field in m s^{-1} for the 0.81 sigma level superimposed. The vertical coordinate sigma is the terrain following vertical height represented as pressure over the surface pressure. This figure uses data obtained from the study which contributed to *Reid and Budd* [1995] and *Budd et al*. [1995].

cipitation at high latitudes as a result of global warming. An increase in freshwater flux into the open ocean in the form of precipitation would increase the stability of the surface ocean layers, thereby enhancing sea-ice production [*Fichefet and Morales Maqueda*, 1999] and increasing the ice thickness by inhibiting deep-ocean convection and the upwelling of warmer deep waters [*Martinson and Iannuzzi*, 1998]. The increased contribution of snow-ice formation may also lead to a significantly modified brine rejection rate. Under current conditions, a factor contributing to snow-ice formation appears to be the effect of high oceanic heat fluxes in certain regions (e.g., Maud Rise, Weddell Sea, and Ross Sea), leading to basal ice melt or a cessation of thermodynamic basal sea-ice growth [*Ackley et al*., 1995; *Jeffries et al*., 2001]. Work by *Lytle and Ackley* [2001] further suggests that snow-ice basal melt may lead to the continual vertical downward transport of snow ice to melt at the ice base. Such a freshwater flux would, they argue, be sufficient to inhibit deep-ocean convection under certain circumstances.

Eicken et al. [1995] further suggested that an increase in snow flooding would be further enhanced by the increased porosity of the ice due to an increase in its temperature. They suggest that snow loading and flooding would have a particularly large effect within the advancing ice edge zone or early in the growth season by both decreasing ice growth rates and causing enhanced snow-ice formation due to loading on comparatively thin ice. Predicted increases in precipitation in spring-summer may have a significant effect on the amount of ice that survives the austral summer by affecting snow shielding and snow-ice formation [*Eicken et al*., 1995]. This may in turn affect sea-ice extent in the subsequent winter [*Comiso and Gordon*, 1998].

Another significant effect would be on sea-ice microbial communities. A thicker snow cover would reduce the intensity and modify the spectral composition of photosynthetically active radiation [*Sullivan et al*., 1985]. On the other hand, flooding may bring nutrients up to the relatively light ice surface, allowing a community to develop that is to some degree protected from grazing by krill and other larger organisms. A thicker snow layer may afford greater protection from ultraviolet radiation for ice-loving organisms [*Perovich*, 1995].

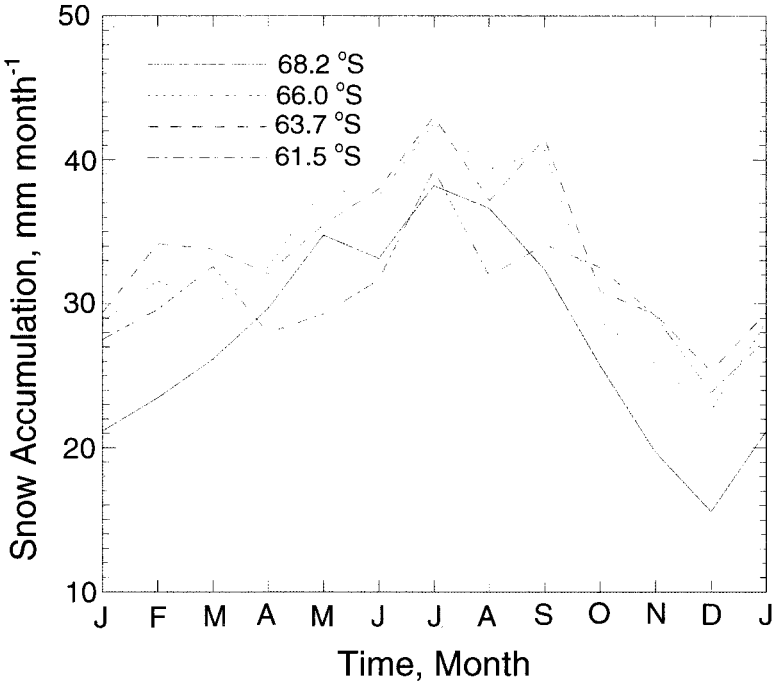

Figure 18. Seasonal cycle of the zonal mean snow accumulation rate (mm month^{-1}) for several latitudes off the Antarctic coast for the period September 1989 to November 1992. This figure uses data obtained from the study which contributed to *Reid and Budd* [1995] and *Budd et al.* [1995].

4. CONCLUSIONS

Recent field programs have greatly improved our understanding of the complex roles of snow in interactions of Antarctic sea ice with the atmosphere, ocean, and biota. Important findings have emerged, including the role of snow in snow-ice formation, lower effective thermal conductivities than are typically used in models, and the fact that significant snowmelt events can affect large areas, even in winter. It is likely that snow will play an increasingly important role if global change increases high-latitude snowfall.

Sturm et al. [1998] observed that the cyclical passage of warm and cold fronts, while producing heterogeneity in winter at scales of <100 km, also produces large-scale homogeneity. Note, for example, how similar the pro-

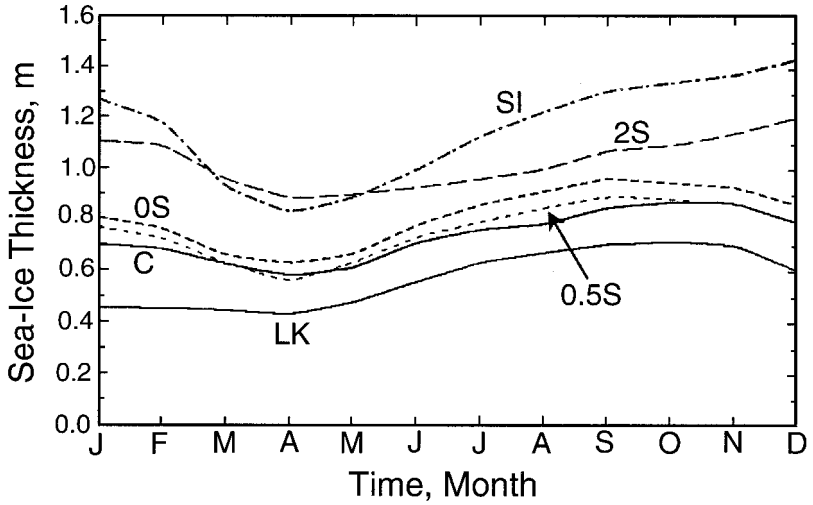

Figure 19. The seasonal cycle of the area-weighted average of Antarctic sea-ice thickness, as modeled by *Wu et al.* [1999]. Curves are labeled as follows: C, control run; SI, ice; 0S, no snow; 0.5S, half as much snowfall on the surface as provided by the original model; 2S, twice as much snowfall as in the original model; and LK, k_{bulk} = 0.164 W m^{-1} K^{-1} (rather than 0.31 W m^{-1} K^{-1}, as used in curve C). Reprinted from Wu et al. [1999] with permission from Springer-Verlag.

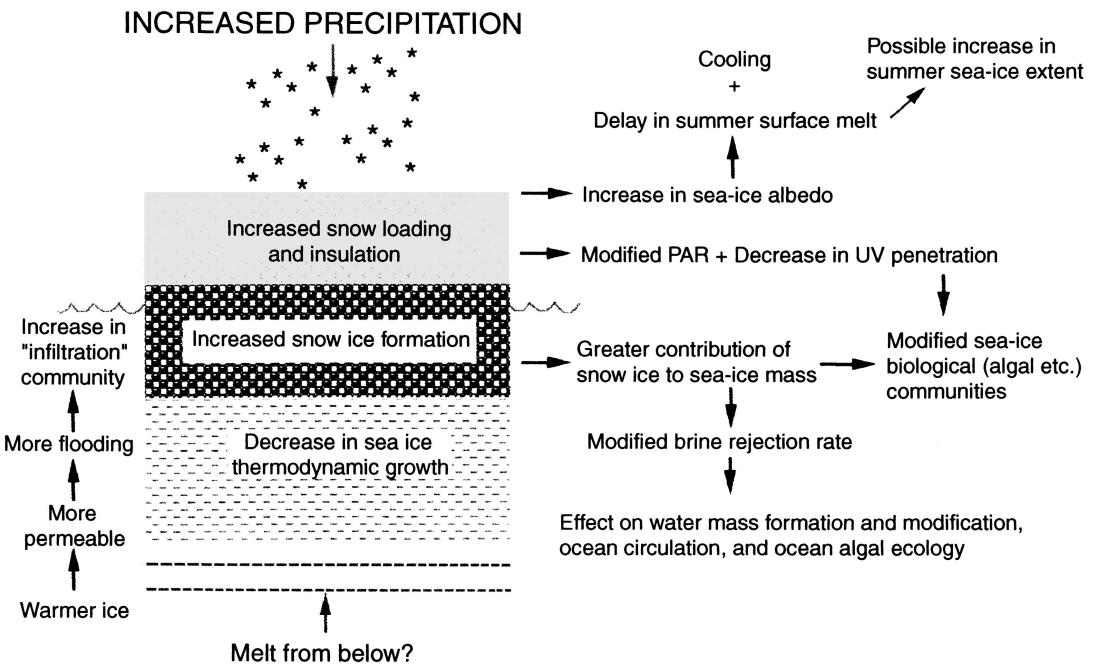

Figure 20. Schematic of the effect on the snow-ice-ocean-atmosphere-biota system of enhanced precipitation due to predicted global warming.

portions of different snow types are from different East Antarctic cruises in Table 3. While point prediction of snow properties is impossible, predictable stratigraphic and textural sequences do develop each winter at the regional scale, with the proportions of depth hoar and icy snow increasing and decreasing, respectively, with increasing latitude (Figure 21). *Sturm et al*. [1998] surmised that periodic flooding and subsequent snow-ice formation effectively diminish the degree to which snow metamorphism processes can create large-scale inhomogeneity in the snowpack as the season progresses.

Significant contrasts exist between the snow covers on sea ice in the two polar regions, suggesting that models need to parameterize snow and ice interactions differently. In the Arctic, snow-ice formation is relatively uncommon (although it may play a significant role in seasonal first-year ice in marginal seas such as the Greenland Sea), and hard wind slabs and depth hoar make up the bulk of the snow cover. Moreover, melt features, while common in the Antarctic even in winter, are rare in the high Arctic until spring. However, Arctic melt commences very rapidly by the end of June, so that the snow and even the top ice layers diminish within a couple of weeks and cover up to 30% of the ice surface [*Tucker et al*., 1992]. In contrast, summer surface melt is only very moderate in the Antarctic. More data are required to better characterize the distribution and properties of snow in summer. Much of the large-scale information on melt extent in the seasonal sea-ice zone has been inferred from satellite radar remote sensing [*Drinkwater and Liu*, 2000].

Other significant gaps remain in our understanding of snow processes. For example, improved accumulation data are required to validate global circulation models and to resolve spatial and temporal variability. This is a difficult task in the windy Antarctic environment, and much reliance will continue to be placed on improved modeling using the best available meteorological data as input. Further modeling is required to determine the role of aeolian redistribution and loss by sublimation and the role of crusts in locking snow in place. Sublimation of blowing snow can lead to significant episodic vertical and horizontal fluxes of water and energy [*Déry et al*., 1998; *Pomeroy and Gray*, 1994], which are not presently incorporated in models.

Snow is currently represented in a simplistic fashion in numerical sea ice–climate models, in terms of both its thickness distribution and properties. Given the rapid metamorphism that occurs in snow on Antarctic sea ice, and the effect this has on the effective thermal conductivity, time-dependent changes in snow parameters should ideally be included in models, in addition to changes in snow thickness. Similarly, ocean swell penetration plays a significant role in modifying and even removing the snow cover in the outer pack ice. Again, such processes are not included in present models, due in part to their complexity. Given their importance, snow-ice formation processes should also be included in large-scale modeling of Antarctic sea ice, with models taking into account energetic constraints (i.e., strict conservation of mass and energy) for freezing of a flooded snow layer.

Measured values of the bulk effective thermal conductivity of snow are lower than those currently pre-

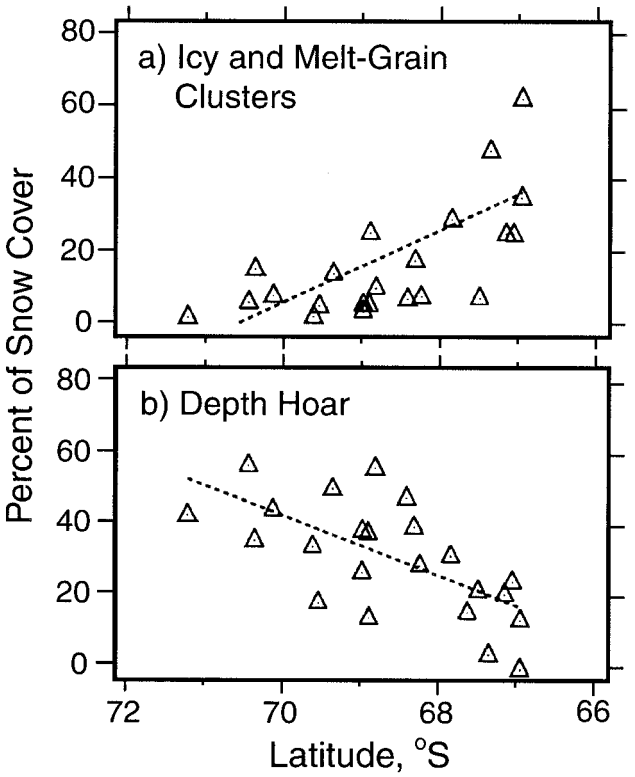

Figure 21. Differences in the proportions of (a) icy snow and (b) depth hoar with latitude. These data are from snow pits in the Amundsen and Ross Seas in the winter of 1994. After *Sturm et al*. [1998].

scribed in models. In a recent Arctic experiment, *Sturm et al*. [2001] derived a similarly low value. However, after comparing the heat flux computed from ice growth rates with that computed from temperature gradients in the snow, they suggest that the bulk value is too low if the snow cover is treated like a homogeneous layer to which a one-dimensional conductive heat flow model is applied. *Sturm et al*. [2001] argue that lateral as well as vertical heat flow is common, resulting in the development of areas of concentrated heat loss at the snow and ice surface, and increasing the effective conductivity of the snow by a factor of 1.4 when aggregated over large areas. This accounts for some of the discrepancy in heat fluxes, while nonconductive heat-transfer mechanisms, like natural and forced air convection, may also increase k_{bulk}. Further work is necessary, as lower values have important implications in the computation of thermodynamic ice growth and salt rejection rates. Difficulty remains in reconciling the difference in scales involved, i.e., between direct measurements of thermal conductivity and those heat-transfer processes addressed by models, which operate at a significantly larger scale.

Present computations of salt flux into the underlying ocean take no account of salt rejected upward and stored in the "blotting pad" of snow and the effect this has on the ocean stability. Moreover, the effect of the release of this salt at summer melt on high-latitude ecosystems and the structure of the oceanic mixed layer is unknown. Thermodynamic effects of a snow cover on ice connectivity, brine channel formation, brine volume, and ice porosity, and their variability, are complex and poorly understood, although progress is being made [e.g., *Golden et al*., 1998; *Maksym and Jeffries*, 2000].

Regarding snow thickness, an effort to systematically and regularly record snow (and ice) thickness along regularly spaced meridional transects by ship has recently been initiated within the Scientific Committee on Antarctic Research (SCAR) Antarctic Sea-Ice Processes and Climate (ASPeCt) program [*Worby and Ackley*, 2000]. While promising efforts have recently been made to derive circumpolar snow thickness distributions remotely from satellite passive microwave data [e.g., *Arrigo et al*., 1996; *Markus and Cavalieri*, 1998], more independent data are required for validation under a range of seasons and conditions. Once validated, such data will improve our understanding of possible links between spatial patterns of snow-ice formation and regional patterns in snow depth.

In addition to collecting data along specified cruise transects where possible, future experiments should ideally be designed to resolve temporal variability in snow cover properties, including microwave signature. In particular, more work is required to estimate the regional and seasonal contribution of snow ice to the overall mass balance of the Antarctic pack. As *Jeffries et al*. [1998b] point out, the occurrence of flooding and snow-ice formation is a complex function of the interplay between snow accumulation and redistribution, basal ice growth and melt, and the temperature-dependent ice permeability and porosity. Such experiments may best be carried out from drifting ice camps.

Finally, observations suggest that the accurate retrieval of sea-ice geophysical parameters (e.g., ice concentration) from satellite microwave data requires a better understanding of the role of snow and the significant differences in conditions between the Antarctic and Arctic. A wet or aging and metamorphosing snow cover makes a significant contribution to the observed variance in both the radiometric brightness temperature [*Comiso et al*., 1992] and radar backscatter of sea ice [*Hallikainen and Winebrenner*, 1992].

ACKNOWLEDGMENTS. The authors are very grateful to the captains, crews, and helicopter pilots on the R/Vs *Aurora Australis*, *Nathaniel B. Palmer*, *Polarstern*, and *Icebird* and to a great number of field assistants on the various cruises, who are unfortunately far too numerous to list here. R.M. thanks Joey Comiso of NASA Goddard Space Flight Center for his support during WWGS '92 and the Alfred-Wegener-Institut für Polar- und Meeresforschung, the U.S. National Research Council, and the National Science Foundation. The contributions of Jeffries, Morris, and Sturm were made possible by NSF-OPP grants 9117211, 9316767, and 9614844, Edison Chouest Offshore, and Antarctic Support Associates personnel. M.R.D. completed this work at the Jet Propulsion Laboratory, Califor-

nia Institute of Technology, under contract to NASA code YS with grant 665.21.02. S.W. acknowledges support by NSF grant OPP-98-15156. We thank Peter Cargill and two anonymous reviewers for their excellent suggestions, the editor James Smith, and Bill Budd of the Antarctic CRC. This paper is dedicated to the memory of our friend and colleague Al Lohanick.

Thomas Torgersen was the Editor responsible for this paper. He thanks Andreas Edgar and an anonymous reviewer for technical reviews and Peter Cargill for the cross-disciplinary review.

REFERENCES

Ackley, S. F., and C. W. Sullivan, Physical controls on the development and characteristics of Antarctic sea ice biological communities—A review and synthesis, *Deep Sea Res*., *Part I*, *41*(10), 1583–1604, 1994.

Ackley, S. F., M. A. Lange, and P. Wadhams, Snow cover effects on Antarctic sea ice thickness, in *Sea Ice Properties and Processes, CRREL Monogr. 90-1*, edited by S. F. Ackley and W. F. Weeks, pp. 16–21, U.S. Army Corps of Eng., Hanover, N. H., 1990.

Ackley, S. F., V. I. Lytle, G. A. Kuehn, K. M. Golden, and M. N. Darling, Sea-ice measurements during ANZFLUX, *Antarct. J. U. S*., *30*(5), 133–135, 1995.

Akitaya, E., Studies of depth hoar, *Low Temp. Sci*., *Ser. A*, *26*, 1–67, 1974.

Allison, I., and A. P. Worby, Seasonal changes of sea-ice characteristics off East Antarctica, *Ann. Glaciol*., *20*, 195–201, 1994.

Allison, I., R. E. Brandt, and S. G. Warren, East Antarctic sea ice: Albedo, thickness distribution, and snow cover, *J. Geophys. Res*., *98*(C7), 12,417–12,429, 1993.

Anderson, D. L., The physical constants of sea ice, *Research*, *13*, 310–318, 1960.

Andreas, E. L., Heat and moisture advection on Antarctic sea ice, *Mon. Weather Rev*., *113*(5), 736–746, 1985.

Andreas, E. L., A theory for the scalar roughness and the scalar transfer coefficients over snow and sea ice, *Boundary Layer Meteorol*., *38*, 159–184, 1987.

Andreas, E. L., Air-ice drag coefficients in the western Weddell Sea, 2, A model based on form drag and drifting snow, *J. Geophys. Res*., *100*(C3), 4833–4843, 1995.

Andreas, E. L., and S. F. Ackley, On the differences in ablation seasons of Arctic and Antarctic sea ice, *J. Atmos. Sci*., *389*, 440–447, 1982.

Andreas, E. L., and K. J. Claffey, Air-ice drag coefficients in the western Weddell Sea, 1, Values deduced from profile measurements, *J. Geophys. Res*., *100*(C3), 4821–4831, 1995.

Andreas, E. L., M. A. Lange, S. F. Ackley, and P. Wadhams, Roughness of Weddell Sea ice and estimates of the air-ice drag coefficient, *J. Geophys. Res*., *98*(C7), 12,439–12,452, 1993.

Armstrong, R. L., An analysis of compressive strain in adjacent temperature-gradient and equi-temperature layers in a natural snow cover, *J. Glaciol*., *26*(94), 283–289, 1980.

Arrigo, K. R., G. L. van Dijken, and J. C. Comiso, Estimating the thickness of sea ice snow cover in the Weddell Sea from passive microwave brightness temperatures, *NASA Tech. Memo*., *104640*, 20 pp., 1996.

Benson, C. S., and M. Sturm, Structure and wind transport of seasonal snow on the Arctic slope of Alaska, *Ann. Glaciol*., *18*, 261–267, 1993.

Brandt, R. E., and S. G. Warren, Temperature measurements and heat transfer in near-surface snow at the South Pole, *J. Glaciol*., *43*(144), 339–351, 1997.

Brandt, R. E., C. S. Roesler, and S. G. Warren, Spectral albedo, absorptance, and transmittance of Antarctic sea ice, in *Proceedings of the Fifth Conference on Polar Meteorology and Oceanography*, pp. 456–459, Am. Meteorol. Soc., Boston, Mass., 1999.

Budd, W. F., P. A. Reid, and L. J. Minty, Antarctic moisture flux and net accumulation from global atmospheric analyses, *Ann. Glaciol*., *21*, 149–156, 1995.

Clarke, D. B., and S. F. Ackley, Physical, chemical and biological properties of winter sea ice in the Weddell Sea, *Antarct. J. U. S*., *17*(5), 107–109, 1982.

Colbeck, S. C., An overview of seasonal snow metamorphism, *Rev. Geophys*., *20*(1), 45–61, 1982.

Colbeck, S. C., Statistics of coarsening in water-saturated snow, *Acta Metall*., *34*, 347–352, 1986.

Colbeck, S. C., The layered character of snow covers, *Rev. Geophys*., *29*(1), 81–96, 1991.

Colbeck, S., E. Akitaya, R. Armstrong, H. Gubler, J. Lafeuille, K. Lied, D. McClung, and E. Morris, *The International Classification for Seasonal Snow on the Ground*, 23 pp., Int. Comm. on Snow and Ice of the Int. Assoc. of Sci. Hydrol., Gentbrugge, Belgium, 1990.

Comiso, J. C., Sea ice effective microwave emissivities from satellite passive microwave and infrared observations, *J. Geophys. Res*., *88*(C12), 7686–7704, 1983.

Comiso, J. C., and A. L. Gordon, Interannual variability in summer sea ice minimum, coastal polynyas and bottom water formation in the Weddell Sea, in *Antarctic Sea Ice: Physical Processes, Interactions and Variability, Antarct. Res. Ser*., vol. 74, edited by M. O. Jeffries, pp. 293–315, AGU, Washington, D. C., 1998.

Comiso, J. C., and C. W. Sullivan, Satellite microwave and in situ observations of the Weddell Sea ice cover and its marginal ice zone, *J. Geophys. Res*., *91*(C8), 9663–9681, 1986.

Comiso, J. C., T. C. Grenfell, M. Lange, A. W. Lohanick, R. K. Moore, and P. Wadhams, Microwave remote sensing of the Southern Ocean ice cover, in *Microwave Remote Sensing of Sea Ice, Geophys. Monogr. Ser*., vol. 68, edited by F. Carsey, pp. 243–259, AGU, Washington, D. C., 1992.

Cox, G. F. N., and W. F. Weeks, Brine drainage and initial salt entrapment in sodium chloride ice, *CRREL Res. Rep*. *354*, U.S. Army Corps of Eng., Hanover, N. H., 1975.

Crocker, G. B., and P. Wadhams, Modelling Antarctic fast-ice growth, *J. Glaciol*., *35*(119), 3–8, 1989.

Cullather, R. I., D. H. Bromwich, and M. L. Van Woert, Spatial and temporal variability of Antarctic precipitation from atmospheric methods, *J. Clim*., *11*(3), 334–367, 1998.

Danielson, A. L., and M. O. Jeffries, Small-scale variability of physical properties and structural characteristics of a single ice floe, *Antarct. J. U. S*., *27*(5), 85–87, 1992.

Déry, S. J., P. A. Taylor, and J. B. Xiao, Thermodynamic effects of sublimating, blowing snow in the atmospheric boundary layer, *Boundary Layer Meteorol*., *89*, 251–283, 1998.

Drinkwater, M. R., Applications of SAR measurements in ocean-ice-atmosphere interaction studies, in *Oceanographic Applications of Remote Sensing*, edited by M. Ikeda and F. W. Dobson, pp. 391–406, CRC Press, Boca Raton, Fla., 1995.

Drinkwater, M. R., and G. B. Crocker, Modelling changes in the dielectric and scattering properties of young snow-covered ice at GHz frequencies, *J. Glaciol*., *34*(118), 274–282, 1988.

Drinkwater, M. R., and C. Haas, Snow, sea-ice and radar observations during ANT X/4: Summary data report, *Ber. aus dem Fachber. Phys*., *53*, 58 pp., Alfred-Wegener-Inst. für Polar- und Meeresforschung, Bremerhaven, Germany, 1994.

Drinkwater, M. R., and X. Liu, Seasonal to interannual variability in Antarctic sea-ice surface melt, *IEEE Trans. Geosci. Remote Sens.*, *38*(4), 1827–1842, 2000.

Drinkwater, M. R., and V. Lytle, ERS-1 SAR and field-observed austral fall freeze-up in the Weddell Sea, Antarctica, *J. Geophys. Res.*, *102*(C6), 12,593–12,608, 1997.

Drinkwater, M. R., D. G. Long, and D. S. Early, Enhanced resolution scatterometer imaging of Southern Ocean sea ice, *ESA J.*, *17*, 307–322, 1993.

Drinkwater, M. R., R. Hosseinmostafa, and P. Gogineni, C-band backscatter measurements of winter sea ice in the Weddell Sea, Antarctica, *Int. J. Remote Sens.*, *16*(17), 3365–3389, 1995.

Drinkwater, M. R., X. Liu, and D. Low, Interannual variability in Weddell Sea ice from ERS wind scatterometer, in *Proceedings of the International Geoscience and Remote Sensing Symposium (IGARSS '98)*, *Seattle, Washington, July 6–10, 1998*, vol. 4, pp. 1982–1984, Inst. of Electr. and Electron. Eng., New York, 1998.

Eicken, H., The role of sea ice in structuring Antarctic ecosystems, *Polar Biol.*, *12*(1), 3–13, 1992.

Eicken, H., Deriving modes and rates of ice growth in the Weddell Sea from microstructural, salinity and stable-isotope data, in *Antarctic Sea Ice: Physical Properties and Processes, Antarct. Res. Ser.*, vol. 74, edited by M. O. Jeffries, pp. 89–122, AGU, Washington D. C., 1998.

Eicken, H., M. A. Lange, H.-W. Hubberton, and P. Wadhams, Characteristics and distribution patterns of snow and meteoric ice in the Weddell Sea and their contribution to the mass balance of sea ice, *Ann. Geophys.*, *12*(1), 80–93, 1994.

Eicken, H., H. Fischer, and P. Lemke, Effects of the snow cover on Antarctic sea ice and potential modulation of its response to climate change, *Ann. Glaciol.*, *21*(1), 369–376, 1995.

Fahrbach, E., M. Knoche, and G. Rohardt, An estimate of water mass transformation in the southern Weddell Sea, *Mar. Chem.*, *35*(1–4), 25–44, 1991.

Fedotov, V. I., N. V. Cherepanov, and K. P. Tyshko, Some features of the growth, structure and metamorphism of East Antarctic landfast sea ice, in *Antarctic Sea Ice: Physical Processes, Interactions and Variability, Antarct. Res. Ser.*, vol. 74, edited by M. O. Jeffries, pp. 343–354, AGU, Washington, D. C., 1998.

Fichefet, T., and M. A. Morales Maqueda, Modelling the influence of snow accumulation and snow-ice formation on the seasonal cycle of the Antarctic sea-ice cover, *Clim. Dyn.*, *15*(4), 251–268, 1999.

Fichefet, T., B. Tartinville, and H. Goosse, Sensitivity of the Antarctic sea ice to the thermal conductivity of snow, *Geophys. Res. Lett.*, *27*, 401–404, 2000.

Fisher, R., and V. I. Lytle, Atmospheric drag coefficients of Weddell Sea ice computed from roughness profiles, *Ann. Glaciol.*, *27*, 455–460, 1998.

Fritsen, C. H., V. I. Lytle, S. F. Ackley, and C. W. Sullivan, Autumn bloom of Antarctic pack-ice algae, *Science*, *266* (5186), 782–784, 1994.

Garrity, C., Characterization of snow on floating ice and case studies of brightness temperature changes during the onset of melt, in *Microwave Remote Sensing of Sea Ice*, *Geophys. Monogr. Ser.*, vol. 68, edited by F. Carsey, pp. 313–328, AGU, Washington, D. C., 1992.

Gloersen, P., W. J. Campbell, D. J. Cavalieri, J. C. Comiso, C. L. Parkinson, and H. J. Zwally, Arctic and Antarctic sea ice, 1978–1987: Satellite passive-microwave observations and analysis, *NASA Spec. Publ.*, *SP-511*, 290 pp., 1992.

Golden, K. M., S. F. Ackley, and V. I. Lytle, The percolation phase transition in sea ice, *Science*, *282*(5397), 2238–2241, 1998.

Goodwin, I. D., Snow accumulation and surface topography in the katabatic zone of eastern Wilkes Land, Antarctica, *Antarct. Sci.*, *2*(3), 235–242, 1990.

Gordon, A. L., Seasonality of Southern Ocean sea ice, *J. Geophys. Res.*, *86*(C5), 4193–4197, 1981.

Gordon, A. L., and B. A. Huber, Southern Ocean winter mixed layer, *J. Geophys. Res.*, *95*(C7), 11,655–11,672, 1990.

Gow, A. J., On the accumulation and seasonal stratification of snow at the South Pole, *J. Glaciol.*, *5*(40), 467–477, 1965.

Gow, A. J., and S. Epstein, On the use of stable isotopes to trace the origins of ice in a floating ice tongue, *J. Geophys. Res.*, *77*(33), 6552–6557, 1972.

Gow, A. J., and W. B. Tucker III, Sea ice in the polar regions, in *Polar Oceanography: Part A*, *Physical Science*, edited by W. O. Smith, pp. 47–122, Academic, San Diego, Calif., 1990.

Gow, A. J., S. F. Ackley, K. R. Buck, and K. M. Golden, Physical and structural characteristics of Weddell Sea pack ice, *Rep. 87-14*, 70 pp., U.S. Army Cold Regions Res. and Eng. Lab., Hanover, N. H., 1987.

Granberg, H. B., Snow cover on sea ice, in *Physics of Ice-Covered Seas*, vol. 1, edited by M. Leppäranta, pp. 605–649, Helsinki Univ. Press, Helsinki, 1998.

Grenfell, T. C., Theoretical model of the optical properties of sea ice in the visible and near infrared, *J. Geophys. Res.*, *88*(C4), 9723–9735, 1983.

Grenfell, T. C., and S. G. Warren, Representation of a nonspherical ice particle by a collection of independent spheres for scattering and absorption of radiation, *J. Geophys. Res.*, *104*(D24), 31,697–31,709, 1999.

Grenfell, T. C., S. G. Warren, and P. C. Mullen, Reflection of solar radiation by the Antarctic snow surface at ultraviolet, visible, and near-infrared wavelengths, *J. Geophys. Res.*, *99*(D9), 18,669–18,684, 1994.

Guest, P. S., and K. L. Davidson, Factors affecting variations of snow surface temperature and air temperature over sea ice in winter, in *The Polar Oceans and Their Role in Shaping the Global Environment, Geophys. Monogr. Ser.*, vol. 85, edited by O. M. Johannessen, R. D. Muench, and J. E. Overland, pp. 435–442, AGU, Washington, D. C., 1994.

Haas, C., The seasonal cycle of ERS scatterometer signatures over perennial Antarctic sea ice and associated surface ice properties and processes, *Ann. Glaciol.*, in press, 2001.

Haas, C., T. Viehoff, and H. Eicken, Sea-ice conditions during the Winter Weddell Gyre Study 1992 ANT X/4 with RV "*Polarstern*": Shipboard observations and AVHRR satellite imagery, *Ber. aus dem Fachber. Phys.*, *34*, 85 pp., Alfred-Wegener-Inst. für Polar- und Meeresforschung, Bremerhaven, Germany, 1992.

Haas, C., H. Rebhan, D. N. Thomas, and T. Viehoff, Sea ice, in *The Expedition ANTARKTIS-XI/3 of RV "Polarstern"*, edited by H. Miller and H. Grobe, Report on polar research, *188/96*, pp. 29–43, Alfred-Wegener-Inst. für Polar- und Meereforschung, Bremerhaven, Germany, 1996.

Haas, C., D. N. Thomas, M. Steffens, and J. Bareiss, Physical and biological investigations of sea-ice, in *The Expedition ANTARKTIS-XIV of RV "Polarstern" in 1997, Report of Leg ANT-XIV/3*, edited by W. Jokat and H. Oerter, Report on polar research, *267/98*, pp. 18–30, Alfred-Wegener-Inst. für Polar- und Meereforschung, Bremerhaven, Germany, 1998.

Haas, C., D. N. Thomas, and J. Bareiss, Surface properties and processes of perennial Antarctic sea ice in summer, *J. Glaciol.*, in press, 2001.

Hallikainen, M., and D. P. Winebrenner, The physical basis for sea ice remote sensing, in *Microwave Remote Sensing of Sea Ice, Geophys. Monogr. Ser.*, vol. 68, edited by F. Carsey, pp. 29–46, AGU, Washington, D. C., 1992.

Hibler, W. D., III, A dynamic thermodynamic sea ice model, *J. Phys. Oceanogr.*, *9*(4), 815–846, 1979.

Holt, B., and S. A. Digby, Processes and imagery of first-year

fast sea ice during the melt season, *J. Geophys. Res*., *90*(C3), 5045–5062, 1985.

Hunt, B. G., H. B. Gordon, and H. L. Davies, The impact of the greenhouse effect on sea-ice characteristics and snow accumulation in the polar regions, *Int. J. Climatol*., *15*(1), 3–23, 1995.

Jeffries, M. O., Describing the composition of sea-ice cores and the development of the Antarctic sea ice cover, *Antarct. J. U.S*., *XXXII*(5), 55–56, 1997.

Jeffries, M. O., and U. Adolphs, Early winter snow and ice thickness distribution, ice structure and development of the western Ross Sea pack ice between the ice edge and the Ross Ice Shelf, *Antarct. Sci*., *9*(2), 188–200, 1997.

Jeffries, M. O., and K. Morris, Salinity of sea ice and snow in early winter 1995 and 1998 in the Ross Sea, *Antarct. J. U. S*., in press, 2001.

Jeffries, M. O., and W. F. Weeks, Structural characteristics and development of sea ice in the western Ross Sea, *Antarct. Sci*., *5*(11), 63–75, 1993.

Jeffries, M. O., R. A. Shaw, K. Morris, A. L. Veazey, and H. R. Krouse, Crystal structure, stable isotopes ($\delta^{18}O$), and development of sea ice in the Ross, Amundsen, and Bellingshausen Seas, *J. Geophys. Res*., *99*(C1), 985–995, 1994a.

Jeffries, M. O., A. L. Veazey, K. Morris, and H. R. Krouse, Depositional environment of the snow cover on West Antarctic pack-ice floes, *Ann. Glaciol*., *20*, 33–38, 1994b.

Jeffries, M. O., A. P. Worby, K. Morris, and W. F. Weeks, Seasonal variations in the properties, and structural and isotopic composition of sea ice and snow cover in the Bellingshausen and Amundsen Seas, Antarctica, *J. Glaciol*., *43*(143), 138–151, 1997a.

Jeffries, M. O., A. P. Worby, K. Morris, W. F. Weeks, B. Hurst-Cushing, R. Jaña, and H. R. Krouse, Late winter snow and ice characteristics of first-year floes in the Bellingshausen and Amundsen Seas, Antarctica: Results of investigations during R.V. *Nathaniel B. Palmer* cruise NBP 93-5 in August and September 1993, *Rep. UAG-R-325*, Geophys. Inst., Univ. of Alaska Fairbanks, 1997b.

Jeffries, M. O., S. Li, R. A. Jaña, H. R. Krouse, and B. Hurst-Cushing, Late winter first-year ice floe thickness variability, seawater flooding and snow ice formation in the Amundsen and Ross Seas, in *Antarctic Sea Ice: Physical Processes, Interactions and Variability, Antarct. Res. Ser*., vol. 74, edited by M. O. Jeffries, pp. 69–88, AGU, Washington, D. C., 1998a.

Jeffries, M. O., B. Hurst-Cushing, H. R. Krouse, and T. Maksym, The role of snow in the thickening and mass budget of first-year floes in the eastern Pacific sector of the Antarctic pack ice, *Rep. UAG-R-327*, Geophys. Inst., Univ. of Alaska Fairbanks, 1998b.

Jeffries, M. O., H. R. Krouse, B. Hurst-Cushing, and T. Maksym, Snow ice accretion and snow cover depletion on Antarctic first-year sea ice floes, *Ann. Glaciol*., in press, 2001.

Jordan, R., A one-dimensional temperature model for a snow cover: Technical documentation for SNTHERM.89, *CRREL Spec. Rep*. *91-16*, U.S. Army Corps of Eng., Hanover, N. H., 1991.

Kawamura, T., T. Takizawa, K. I. Ohshima, and S. Ushio, Data of sea-ice cores obtained in Lützow-Holm Bay from 1990 to 1992 (JARE-31, -32) in the period of Japanese Antarctic climate research, *JARE Data Rep. 204* (*Glaciol. 24*), 42 pp., Natl. Inst. of Polar Res., Tokyo, 1995.

Kawamura, T., K. Ohshima, T. Takizawa, and S. Ushio, Physical, structural and isotopic characteristics and growth processes of fast ice in Lützow-Holm Bay, Antarctica, *J. Geophys. Res*., *102*(C2), 334–355, 1997.

Lang, R. M., B. R. Leo, and R. L. Brown, Observations on the growth process and strength characteristics of surface hoar, in *Proceedings of the International Snow Science Workshop*, pp. 188–195, Int. Snow Sci. Workshop Comm., Aspen, Colo., 1984.

Lange, M., and H. Eicken, The sea ice thickness distribution in the northwestern Weddell Sea, *J. Geophys. Res*., *96*(C3), 4821–4837, 1991.

Lange, M., and H.-W. Hubberten, Isotopic composition of sea ice as a tool for understanding sea ice processes in the polar regions, in *Physics and Chemistry of Ice*, edited by N. Maeno and T. Hondoh, pp. 399–405, Hokkaido Univ. Press, Sapporo, Japan, 1992.

Lange, M. A., P. Schlosser, S. F. Ackley, P. Wadhams, and G. S. Dieckmann, ^{18}O concentrations in sea ice of the Weddell Sea, Antarctica, *J. Glaciol*., *36*(124), 315–323, 1990.

Ledley, T. S., Snow on sea ice: Competing effects in shaping climate, *J. Geophys. Res*., *96*(D9), 17,195–17,208, 1991.

Lohanick, A. W., Some observations of established snow cover on saline ice and their relevance to microwave remote sensing, in *Sea Ice Properties and Processes*, *CRREL Monogr. 90-1*, edited by S. F. Ackley and W. F. Weeks, pp. 61–67, U.S. Army Corps of Eng., Hanover, N. H., 1990.

Lytle, V. I., and S. F. Ackley, Snow properties and surface elevation profiles in the western Weddell Sea (NBP92-2), *Antarct. J. U.S*., *27*(5), 93–94, 1992.

Lytle, V. I., and S. F. Ackley, Heat flux through sea ice in the western Weddell Sea: Convective and conductive transfer processes, *J. Geophys. Res*., *101*(C4), 8853–8868, 1996.

Lytle, V. I., and S. F. Ackley, Snow ice growth: A freshwater flux inhibiting deep convection in the Weddell Sea, Antarctica, *Ann. Glaciol*., in press, 2001.

Maksym, T., and M. O. Jeffries, A one-dimensional percolation model of flooding and snow ice formation with particular reference to sea ice in the Ross Sea, Antarctica, *J. Geophys. Res*., *105*(C11), 26,313–26,331, 2000.

Manabe, S., R. J. Stouffer, M. J. Spelman, and K. Bryan, Transient responses of a coupled ocean-atmosphere model to gradual changes of atmospheric CO_2, part I, Annual mean response, *J. Clim*., *4*(8), 785–818, 1991.

Marbouty, D., An experimental study of temperature gradient metamorphism, *J. Glaciol*., *26*(94), 303–312, 1980.

Markus, T., and D. J. Cavalieri, Snow depth distribution over sea ice in the Southern Ocean from satellite passive microwave data, in *Antarctic Sea Ice: Physical Processes, Interactions and Variability, Antarct. Res. Ser*., vol. 74, edited by M. O. Jeffries, pp. 19–39, AGU, Washington, D.C., 1998.

Martinson, D. G., and R. A. Iannuzzi, Antarctic ocean-ice interaction: Implications from ocean bulk property distributions in the Weddell Gyre, in *Antarctic Sea Ice Physical Processes, Interactions and Variability, Antarct. Res. Ser*., vol. 74, edited by M. O. Jeffries, pp. 243–271, AGU, Washington, D.C., 1998.

Massom, R. A., Observing the advection of sea ice in the Weddell Sea using buoy and satellite passive microwave data, *J. Geophys. Res*., *97*(C10), 15,559–15,572, 1992.

Massom, R. A., M. R. Drinkwater, and C. Haas, Winter snow cover on sea ice in the Weddell Sea, *J. Geophys. Res*., *102*(C1), 1101–1117, 1997.

Massom, R. A., V. I. Lytle, A. P. Worby, and I. Allison, Winter snow cover variability on East Antarctic sea ice, *J. Geophys. Res*., *103*(C11), 24,837–24,855, 1998.

Massom, R. A., J. C. Comiso, A. P. Worby, V. I. Lytle, and L. Stock, Regional classes of sea ice cover in the East Antarctic pack observed from satellite and in situ data during a winter time period, *Remote Sens. Environ*., *68*(1), 61–76, 1999.

Mätzler, C., E. Schanda, and W. Good, Towards the definition of optimum sensor specifications for microwave remote

sensing of snow, *IEEE Trans. Geosci. Remote Sens*., *GE-20*(1), 57–66, 1982.

Maykut, G. A., The surface heat and mass balance, in *The Geophysics of Sea Ice*, edited by N. Untersteiner, *NATO ASI Ser*., *Ser. B*, *146*, 395–463, Plenum, New York, 1986.

Maykut, G. A., and N. Untersteiner, Some results from a time-dependent thermodynamic model of sea ice, *J. Geophys. Res*., *76*(6), 1550–1575, 1971.

McPhee, M. G., S. F. Ackley, P. Guest, B. A. Huber, D. G. Martinson, J. H. Morison, R. D. Muench, L. Padman, and T. P. Stanton, The Antarctic Zone Flux Experiment, *Bull. Am. Meteorol. Soc*., *77*, 1221–1232, 1996.

Meese, D. A., J. W. Govoni, and S. F. Ackley, Snow and sea-ice thicknesses: Winter Weddell gyre study, 1989, *Antarct. J. U. S*., *25*(5), 118, 1990.

Mitchell, J. F. B., S. Manabe, V. Meleshko, and T. Tokioka, Equilibrium climate change—and its implications for the future, in *Climate Change—The IPCC Scientific Assessment*, edited by J. T. Houghton, G. J. Jenkins, and J. J. Ephraums, pp. 131–172, Cambridge Univ. Press, New York, 1990.

Morris, K., and M. O. Jeffries, Seasonal contrasts in snow cover characteristics on Ross Sea ice floes, *Ann. Glaciol*., in press, 2001.

Morris, K., M. O. Jeffries, and S. Li, Sea ice characteristics and seasonal variability of ERS 1 SAR backscatter in the Bellingshausen Sea, in *Antarctic Sea Ice: Physical Processes, Interactions and Variability, Antarct. Res. Ser*., vol. 74, edited by M. O. Jeffries, pp. 213–242, AGU, Washington, D. C., 1998.

Oelke, C., Atmospheric signatures in sea-ice concentration estimates from passive microwaves: Modelled and observed, *Int. J. Remote Sens*., *18*(5), 1113–1136, 1997.

Onstott, R. G., and S. P. Gogineni, Active microwave measurements of Arctic sea ice under summer conditions, *J. Geophys. Res*., *90*(C3), 5035–5044, 1985.

Paige, R. A., and C. W. Lee, Preliminary studies of sea ice in McMurdo Sound, Antarctica, during "Deep Freeze 65," *J. Glaciol*., *6*(46), 515–528, 1967.

Perovich, D. K., Observations of ultraviolet light reflection and transmission by first-year sea ice, *Geophys. Res. Lett*., *22*(11), 1349–1352, 1995.

Perovich, D. K., Optical properties of sea ice, in *Physics of Ice-Covered Seas*, vol., edited by M. Leppäranta, pp. 195–230, Dep. of Geophys., Univ. of Helsinki, Helsinki, 1998.

Perovich, D. K., and J. A. Richter-Menge, Surface characteristics of sea ice, *J. Geophys. Res*., *99*(C8), 16,341–16,350, 1994.

Petrov, I. G., Ice thickness and snow depth distribution in the coastal part of the Davis Sea, *Sov. Antarct. Exped. Inf. Bull*., *Engl. Transl*., *6*, 305–307, 1967.

Pomeroy, J. W., and D. M. Gray, Sensitivity of snow relocation and sublimation to climate and surface vegetation, in *Snow and Ice Covers: Interactions With the Atmosphere and Ecosystems*, *IAHS Publ*., *223*, edited by H. G. Jones, Int. Assoc. of Hydrol. Sci., Gentbrugge, Belgium, 1994.

Reid, P. A., and W. F. Budd, Calculation of Antarctic surface ice mass accumulation through atmospheric parameters, in *Proceedings of the APOC and AMOS Joint Conference*, Aust. Meteorol. and Oceanogr. Soc., Melbourne, Aust., 1995.

Remund, Q. P., D. G. Long, and M. R. Drinkwater, An iterative approach to multisensor sea-ice classification, *IEEE Trans. Geosci. Remote Sens*., *38*(4), 1843–1856, 2000.

Sommerfeld, R. A., and E. LaChapelle, Classification of snow metamorphism, *J. Glaciol*., *9*(55), 3–17, 1970.

Squire, V. A., P. Wadhams, and S. C. Moore, Surface gravity wave processes in the winter Weddell Sea, *Eos Trans. AGU*, *67*(44), 1005, 1986.

Steffen, K., and T. DeMaria, Surface energy fluxes of Arctic winter sea ice in Barrow Strait, *J. Appl. Meteorol*., *35*(11), 2067–2079, 1996.

Sturm, M., The role of thermal convection in heat and mass transport in the sub-Arctic snow cover, *CRREL Rep*. *91-09*, 84 pp., U.S. Army Corps of Eng., Hanover, N. H., 1991.

Sturm, M., and J. B. Johnson, Thermal conductivity measurements of depth hoar, *J. Geophys. Res*., *97*(B2), 2129–2139, 1992.

Sturm, M., K. Morris, and R. Massom, A description of the snow cover on the winter sea ice of the Amundsen and Ross Seas, *Antarct. J. U. S*., *30*(1–4), 21–24, 1995.

Sturm, M., J. Holmgren, M. Koenig, and K. Morris, The thermal conductivity of seasonal snow, *J. Glaciol*., *43*(143), 26–41, 1997.

Sturm, M., K. Morris, and R. Massom, The winter snow cover of the West Antarctic pack ice: Its spatial and temporal variability, in *Antarctic Sea Ice: Physical Processes, Interactions and Variability, Antarct. Res. Ser*., vol. 74, edited by M. O. Jeffries, pp. 19–40, AGU, Washington, D.C., 1998.

Sturm, M., J. Holmgren, and D. K. Perovich, Spatial variations in the winter heat flux at SHEBA: Estimates from snow-ice interface temperatures, *Ann. Glaciol*., in press, 2001.

Sullivan, C. W., A. C. Palmisano, S. T. Kottmeier, S. McGrath Grossi, and R. Moe, The influence of light on growth and development of the sea-ice microbial community of McMurdo Sound, in *Antarctic Nutrient Cycles and Food Webs*, edited by W. R. Siegfried, P. R. Condy, and R. M. Laws, pp. 84–88, Springer-Verlag, New York, 1985.

Takizawa, T., Characteristics of snow cover on sea ice and formation of snow ice, II, *Low Temp. Sci*., *Ser. A*, *43*, 157–161, 1984.

Tin, T., and M. O. Jeffries, Sea ice thickness and roughness in the Ross Sea, Antarctica, *Ann. Glaciol*., in press, 2001.

Tucker, W. B., III, D. K. Perovich, A. J. Gow, W. F. Weeks, and M. R. Drinkwater, Physical properties of sea ice relevant to remote sensing, in *Microwave Remote Sensing of Sea Ice*, *Geophys. Monogr. Ser*., vol. 68, edited by F. Carsey, pp. 9–28, AGU, Washington, D.C., 1992.

Untersteiner, N., On the mass and heat budget of Arctic sea ice, *Arch. Meteorol. Geophys. Bioklimatol*., *Ser. A*, *12*, 151–182, 1961.

Ushio, S., and T. Takizawa, Oceanographic data in Lützow-Holm Bay of Antarctic Climate Research Programme from March 1990 to January 1991 (JARE-31), *JARE Data Rep. 184 (Glaciol*. *24*), 34 pp., Natl. Inst. of Polar Res., Tokyo, 1993.

Veazey, A. L., M. O. Jeffries, and K. Morris, Small-scale variability of physical properties and structural characteristics of Antarctic fast ice, *Ann. Glaciol*., *20*, 61–66, 1994.

Waddington, E. D., J. Cunningham, and S. L. Harder, Effects of snow ventilation on chemical concentrations, in *Chemical Exchange Between the Atmosphere and Polar Snow*, edited by E. W. Wolff and R. C. Bales, pp. 403–451, *NATO ASI Ser*., *Ser. I*, *43*, Springer-Verlag, New York, 1996.

Wadhams, P., M. A. Lange, and S. F. Ackley, The ice thickness distribution across the Atlantic sector of the Antarctic Ocean in midwinter, *J. Geophys. Res*., *92*(C13), 14,535–14,552, 1987.

Warren, S. G., Optical properties of snow, *Rev. Geophys*., *20*(1), 67–89, 1982.

Warren, S. G., C. S. Roesler, and R. E. Brandt, Solar radiation processes in the East Antarctic sea ice zone, *Antarctic J. U. S*., *32*(5), 185–187, 1997.

Warren, S. G., R. E. Brandt, and P. O. Hinton, Effect of surface roughness on bidirectional reflectance of Antarctic snow, *J. Geophys. Res*., *103*(E11), 25,789–25,807, 1998.

Warren, S. G., I. G. Rigor, N. Untersteiner, V. F. Radionov, N. N. Bryazgin, Y. I. Aleksandrov, and R. Colony, Snow depth on Arctic sea ice, *J. Clim*., *12*, 1814–1829, 1999.

Weeks, W. F., and S. F. Ackley, The growth, structure and properties of sea ice, in *The Geophysics of Sea Ice*, edited by N. Untersteiner, *NATO ASI Ser., Ser. B*, *146*, 9–164, Plenum, New York, 1986.

Winebrenner, D. P., D. G. Long, and B. Holt, Mapping the progression of melt onset and freeze-up on Arctic sea ice using SAR and scatterometry, in *Analysis of SAR Data of the Polar Oceans: Recent Advances*, edited by C. Tsatsoulis and R. Kwok, pp. 129–144, Springer-Verlag, New York, 1998.

Wiscombe, W. J., and S. G. Warren, A model for the spectral albedo of snow, 1, Pure snow, *J. Atmos. Sci.*, *37*(12), 2712–2733, 1980.

Worby, A. P., and S. F. Ackley, Antarctic research yields circumpolar sea-ice thickness data, *Eos Trans. AGU*, *81*(17), 181, 184–185, 2000.

Worby, A. P., and R. A. Massom, The structure and properties of sea ice and snow cover in East Antarctic pack ice, *Res. Rep. 7*, 191 pp., Antarct. Coop. Res. Cent., Hobart, Tasmania, Australia, 1995.

Worby, A. P., N. L. Bindoff, V. I. Lytle, I. Allison, and R. A. Massom, Winter ocean/sea ice interactions studied in the East Antarctic, *Eos*, *77*(46), 453, 456–457, Nov. 12, 1996a.

Worby, A. P., M. O. Jeffries, W. F. Weeks, K. Morris, and R. Jaña, The thickness distribution of sea ice and snow cover during late winter in the Bellingshausen and Amundsen Seas, Antarctica, *J. Geophys. Res.*, *101*(C12), 28,441–28,455, 1996b.

Worby, A. P., R. A. Massom, I. Allison, V. I. Lytle, and P. Heil, East Antarctic sea ice: A review of its structure, properties and drift, in *Antarctic Sea Ice: Physical Processes, Interactions and Variability, Antarct. Res. Ser.*, vol. 74, edited by M. O. Jeffries, pp. 41–68, AGU, Washington, D. C., 1998.

World Meteorological Organization, Sea-ice nomenclature, *WMO/OMM/BMO 259*, *TP. 145*, Geneva, 1971.

Wu, X., W. F. Budd, V. I. Lytle, and R. A. Massom, The effect of snow on Antarctic sea ice simulations in a coupled atmosphere-sea ice model, *Clim. Dyn.*, *15*(2), 127–143, 1999.

Yen, Y. C., Review of thermal properties of snow, ice and sea water, *CRREL Rep. 8–10*, U.S. Army Corps of Eng., Hanover, N. H., 1981.

Zhou, X., S. Li, and K. Morris, Measurement of all-wave and spectral albedo of snow surface on the summer sea ice in the Ross Sea, *Ann. Glaciol.*, in press, 2001.

I. Allison, V. I. Lytle, R. A. Massom, A. P. Worby, and X. Wu, Antarctic Cooperative Research Centre, GPO Box 252-80, University of Tasmania, Hobart, Tasmania 7001, Australia. (R.Massom@utas.edu.au)

M. R. Drinkwater, Oceans/Sea-Ice Unit (APP-FSO), European Space Agency, ESTEC, Keplerlaan 1, Postbus 299, 2200 AG Noordwik, Netherlands.

H. Eicken, M. O. Jeffries, and K. Morris, Geophysical Institute, University of Alaska Fairbanks, 903 Koyukuk Drive, P.O. Box 757320, Fairbanks, AK 99775-7320, USA.

C. Haas, Alfred-Wegener-Institut für Polar-und Meeresforschung, Columbusstrasse, D-27568 Bremerhaven, Germany.

P. A. Reid, Climatic Research Unit, University of East Anglia, Norwich NR4 7TJ, England.

M. Sturm, U. S. Army Cold Regions Research and Engineering Laboratory–Alaska, Fort Wainwright, AK 99703-0170, USA.

S. Ushio, National Institute of Polar Research, 9-10, Kaga 1-Chome, Itabashi-Ku, Tokyo, Japan.

S. G. Warren, Department of Atmospheric Sciences, University of Washington, Box 351640, Seattle, WA 98195, USA.